Understanding the effects of on- and off-hotspot policing: Evidence of hotspot, oscillating and chaotic activities

Nancy Rodríguez* Qi Wang† Lu Zhang‡

March 10, 2021

Abstract

This paper considers a system of partial differential equations that govern the spatio-temporal dynamics of urban crime with law enforcement. The deployment of law enforcement is called on-hotspot policing if the dispatched police approach the crime hotspot gradient with the same intensity as the criminal agents, and it is called off-hotspot policing otherwise. We reveal several parameter regimes governed by the policing intensity that promote the emergence of crime hotspots. The existence and stability of these regular patterns, which can either be time-stationary or time-periodic, are proved using bifurcation theories. The results give a wave mode selection mechanism for these spatially heterogeneous solutions and suggest that hotspot policing can stabilize crime aggregates or drive them from one location to another. We also prove that this PDE system admits a unique and global-in-time solution, and the solution is uniformly bounded. However, this system can be ill-posed for both on- and off-hotspot policing as the solution dynamics do not always change continuously with respect to the initial data. Moreover, phase transitions between closed loops of solution trajectories occur for a wide range of system parameters and this reveals another dimension of complexity of the system. Concerning the anti-hotspot policing strategy (i.e., law enforcement actively deployed away from hotspots in space), we show that this likely counter-intuitive strategy tends to stabilize static hotspots and annihilate time-periodic aggregates. These results point to a difficulty of using this system for something like predicting crime and determining the effectiveness of hotspot policing, due to the parameter sensitivity, and they call for further advancement in the mathematical modeling and analysis of urban criminal activities with hotspot policing.

Keywords: urban crime model, hotspot policing, chaos, pattern formation

*nancy.b.rodriguez@colorado.edu. Department of Applied Mathematics, University of Colorado Boulder, Boulder, CO 80309, United States.

†qwang@swufe.edu.cn. Department of Mathematics, Southwestern University of Finance and Economics, 555 Liutai Ave, Wenjiang, Chengdu, 611130, China. QW is supported by QW thanks Professor Michael Ward at UBC for stimulating discussions. All authors thank the referees for carefully scrutinizing this paper and providing helpful comments which help improve this paper. QW is supported by Sichuan Science and Technology Program (No. 2020YJ0060) and partially by the Fundamental Research Funds for the Central Universities (No. JBK1805001).

‡lz2784@columbia.edu. Department of Applied Physics and Applied Mathematics, Columbia University, New York, NY 10027, United States.

1 Introduction

This paper considers the following system for (A, ρ, u) of space x and time t

$$\begin{cases} A_t = D_A A_{xx} - A + A\rho + \alpha, & x \in (0, L), t > 0, \\ \rho_t = (D_\rho \rho_x - 2\rho A_x/A)_x - A\rho + \beta - u\rho, & x \in (0, L), t > 0, \\ u_t = (D_u u_x - \chi u A_x/A)_x, & x \in (0, L), t > 0, \\ (A, \rho, u)(x, 0) = (A_0, \rho_0, u_0)(x) \geq 0, \not\equiv 0, & x \in (0, L), \\ A_x(x, t) = \rho_x(x, t) = u_x(x, t) = 0, & x = 0, L, t > 0, \end{cases} \tag{1.1}$$

where parameters D_A, D_ρ, D_u α, β and χ are assumed positive constants that will be interpreted later. System (1.1) is a one-dimensional version of a model introduced independently by [41] and [56] to study the spatio-temporal dynamics of urban crime with police influence. Here, the functions A, ρ and u are scalar fields representing the *attractiveness value*, *population density of criminal agents*, and *population density of the dispatched police*, respectively. The main focus of this work is on the emergence and properties of regular (stationary and time-periodic) and irregular (chaotic) spatially heterogeneous solutions of (1.1). In particular, we examine the effects of hotspot policing intensity, measured by the parameter χ, on the pattern formation.

1.1 Model motivation and background

It is widely believed that human behavior is influenced by intrinsically diverse factors and hence does not follow laws similar to those comprising physics and other natural sciences. Moreover, an individual's behavior is too complex to be adequately described by mechanistic models or predicted through quantitative methods. However, at a group level, human behavior can exhibit spatio-temporal regularities which mathematics can help understand. One of the most noticeable examples is the clustering of criminal activity, or the so-called "crime-hotspot", where geographically there are neighborhoods with higher crime rates surrounded by neighborhoods with lower crime rates. Over the past few decades, many works in the social sciences [12, 8, 9, 10, 11] have been devoted to understanding hotspots in criminal activity due to social forces such as social-economic status, security feature, social disorganization, subculture and group conflict, among others. For instance, empirical studies [55, 64, 84] suggest that crime is not spread evenly across city landscapes, but significantly clustered at a much smaller geographic level-the "hot spots", which can generate more than half of all criminal events; moreover, even within the most crime-ridden neighborhoods, crime clusters at a few discrete locations and other areas are relatively crime free [64]. While, in practice, it is unlikely to predict when, where and how crime will take place, historic data of urban burglary demonstrate a persistent and valid pattern illustrating that certain neighborhoods have a higher propensity to crimes than others, even if a crime may occur anywhere in the community.

1.1.1 The model without law enforcement

To shed light on the spatio-temporal dynamics of these crime hotspots, in 2008 a group at UCLA proposed a mathematical model for urban crime in [69]. Grounded on the assumptions of routine activity theory, broken-window effect, and the so-called repeat and near-by repeat victimization effect [2, 28, 14, 40, 70], they build an agent-based lattice model in 2D that incorporates the movement of criminals and the dynamics of the attractiveness value, and the continuum limit of the lattice system is as follows:

$$\begin{cases} A_t = D_A \Delta A - A + A\rho + A^0, \\ \rho_t = \nabla \cdot (D_\rho \nabla \rho - 2\rho \nabla \ln A) - A\rho + \bar{B}. \end{cases} \tag{1.2}$$

Routine activity theory asserts that crime revolves around three factors: a potential offender, a suitable target, and the absence of guardianship [28]. This is related to the so-called broken-window effect, which suggests that signs of neglect, anti-social behavior, and civil disorder can encourage further neglect, destruction, and eventually serious crimes [13, 62, 85]. The repeat and near-repeat victimization effect states that criminal activity in a certain location increases the probability of another crime occurring at the same, or nearby, locations within a short period. This effect has been measured in real-life data for crimes like residential burglaries [40, 70]. The linear diffusion rate, D_A, measures the intensity of the near-repeat victimization effect. Since the expected number of crimes is given by $A\rho$, the self-exciting nature of crime is included in the dynamics by the term "$+A\rho$" in the first equation. When a crime occurs, it is assumed that the agent who committed the crime will return home and be removed from the system, leading to "$-A\rho$" in the second equation. External growth, which can be spatially and temporally heterogeneous, for both unknowns is also assumed, and are represented by A_0 and $\bar{B}$, respectively. Finally, let us mention that the criminal agents move with a combination of linear diffusion (random motion) and a bias towards high attractiveness value (giving rise to the chemotactic-like movement). We refer the interested reader to [32, 69] for the derivation and further justification of (1.2), and to [24, 31] for a review of agent-based urban crime modeling.

Concerning the mathematical analysis, system (1.2) has attracted a substantial amount of academic attention from [4, 5, 6, 7, 15, 16, 30, 50, 44, 49, 48, 67, 69, 73]. These works demonstrate that this system admits rich and complex spatio-temporal dynamics, and the nontrivial patterns studied therein successfully captures the featured crime hotspots of urban residential burglary, presented by dynamical or static concentrating profiles throughout these models. For the time-dependent system (1.2), Rodríguez and Bertozzi [59] established its local well-posedness theory, and Wang *et al.* [78] extended it to the global well-posedness and proved the solution's uniform boundedness in 1D. This model in high-dimensions is studied by [29, 33, 51, 58, 60, 86] with either weak policing intensity or for its modified version with technical conditions assumed.

It is worth noting that (1.2) has been extended in several directions. For instance, in [6, 17, 54] the authors model the criminal dispersal through the Lévy process over Brownian motion. Saldaña *et al.* [61] proposed and studied an age-structured population approach for the mathematical modeling of urban burglaries, while Mohler and Short [52] developed a new framework for geographic profiling based upon Bayes' theorem and kinetic descriptions of criminal behavior. Gu *et al.* [32] considered the spatial heterogeneity of both the near-repeat victimization effect and the dispersal strategy of criminal agents, and harvested a class of reaction-advection-diffusion systems with nonlinear diffusion. Non-trivial patterns in these works also represent the aggregation phenomenon in urban criminal activity.

The introduction of a combination of both random and directed dispersal into populations dynamics has been quite popular in ecology (e.g., species competition, prey-taxis) and biology (e.g., chemotaxis, tumor). We can recognize that (1.2) admits the structure of the Keller–Segel chemotaxis model with logarithmic sensitivity [43], and how criminal agents migrate to favorable targets is very similar to that of chemotaxis cellular organisms direct their movements in response to the gradient of a chemical stimulus. See papers [35, 36] for the surveys on the Keller–Segel chemotaxis models.

1.1.2 The model with law enforcement

Now that crime and disorder are not evenly spread across areas, some crime scholars and practitioners [25, 65, 71, 72, 81, 82] have argued that policing should concentrate in the areas of greatest demand rather than spreading thinly across the urban landscape. This strategy, known as "hot-spot policing" or "hotspotting," is geographically focused, and the location of the crime, rather than the features of criminals, is central to the strategy.

To study the effects of the engagement of law enforcement on the dynamics of criminal activity, [41, 56] independently augmented (1.2) with the following PDE to describe the deployment and focused patrol of the police:

$$u_t = \nabla \cdot (D_u \nabla u - \chi u \nabla \ln A), \tag{1.3}$$

where u denotes the distribution of law enforcement in field. The positive parameters D_u and χ measure the intensity of police's random walk and response to criminal activity, respectively. The additional equation reveals several characteristic features of policing patrolling. First of all, the police neither enter nor leave the PDE system and their total number is conserved. Moreover, in addition to a random patrolling, the policing is informed in part by environmental criminology, and the characteristics of an area or place are viewed as key in explaining clusters of criminal events, however, it is unfair to give the police credit of direct knowledge of the criminal density when deciding where to move, hence move preferably to locations with high attractiveness.

Setting $A_0 \equiv \alpha$ and $\bar{B} \equiv \beta$, we combine (1.2) and (1.3) to collect (1.1). This new class of three-component reaction-advection-diffusion systems has been analyzed by few authors [15, 74]. These works apply a singular perturbation analysis by first constructing stationary hotspot in the limit of large criminal diffusivity and small attractiveness diffusivity and then analyze their linear stability through nonlocal eigenvalue theory, which is conducted for certain χ including the cops-on-the-dot strategy. Additional studies incorporating law enforcement have also provided insights into understanding the effects of police deployment on the formation and annihilation of hotspots. Ricketson [57] extended [41] by considering a variety of policing strategies through the variation in their biased movements. Among other things, it is demonstrated in [57] that among the policing strategies investigated, the one that minimizes the number of crimes committed is not the same as the one the yields the most uniform distribution of crime. This tends to suggests an optimal strategy, which is problematic from the point of view of equity, of tolerating crime over some concentrated regions in order to minimize the total aggregate criminal activity. We would like to mention that rather than incorporating (1.3), [67, 68, 87] model the cops-on-the-dots deployment by introducing a static deterrence profile $d(x)$ to "$-A\rho$" in (1.2).

1.2 Main results

In this work, we explore the complex spatio-temporal dynamics of system (1.1) through rigorous bifurcation analysis complemented with numerical experiments. We find three distinct parameter regimes where the system exhibits dramatically different spatio-temporal dynamics. This high sensitivity to the system parameters points to the difficulty of trying to predict future crime patterns based on fitting the model to previous data. First, we show that the system supports bifurcation in a certain parameter regime. Our analysis applies the steady state bifurcation theory that verifies a branch of spatially heterogenous solutions bifurcating from the constant equilibrium solution. The existence and stability of such said branch of solutions are discussed in Section 3. We find a different parameter regime leading to a branch of time-periodic solutions in Section 4. To our knowledge the only work that had addressed oscillating solutions in such systems was due to [15, 74] where they considered the formation of oscillating patterns out of spatial spikes. To be specific, the spikes therein bifurcate from hotspot constructed in the singular limit of system parameters, therefore their analysis is restricted to $\chi = 2$ or 3 due to technical considerations. This is not the case in this work as we can relax these considerations by studying the bifurcation from the homogeneous state. The analysis of the Hopf bifurcation and the stability of the time-periodic solutions are discussed in Section 4. The stability or instability of these branches can help determine whether perturbations to the system will push the dynamic solution to system (1.1) toward the constant equilibrium or to a displaced hotspot

solution, at least around the bifurcation points. The results in Sections 3 and 4 are weakly nonlinear in the sense that the non-constant solutions discussed there occur for parameters that are close to those leading to the bifurcation from the constant equilibrium solution. To explore what happens away from these bifurcation points, we perform some numerical experiments in Section 5. In fact, away from the bifurcation points, we find a parameter regime that leads to solutions which are unstable with respect to initial data. In this regime, very small variations of the initial data can lead to extremely different behaviors of the corresponding solutions. This is verified numerically through various experiments that illustrate the ill-posed nature of system (1.1) due to the lack of stability with respect to initial data in some parameter regimes. Prototypical solutions to (1.1) in each of the regimes analyzed here, obtained through numerical experiments, are illustrated in Section 5.

Before proceeding further, it seems necessary to mention that one can follow [78] to prove the global existence, uniqueness and boundedness of solution to (1.1). We state them as follows:

Theorem 1.1. *For initial data $(A_0, \rho_0, u_0) \in H^1(0,L)\times H^1(0,L)\times H^1(0,L)$ with $A_0(x) > 0$ and $\rho_0, u_0 \geq, \not\equiv 0$ in $(0,L)$, (1.1) admits a unique classical solution $(A(x,t), \rho(x,t), u(x,t))$ defined on $[0,L]\times[0,\infty)$; Moreover, there exist positive constants C_0 and C_1 such that $C_0 \leq A(x,t) < C_1$ and $0 < \rho(x,t), u(x,t) \leq C_1$ for all $t \in (0,\infty)$.*

Proof. First of all, the local existence and uniqueness of (1.1) with $T_{\max} \leq \infty$ are standard. Then, one has from the strong maximum principle that A, ρ and u are strictly positive in $[0,L]$ for all time $t \in (0, T_{\max})$. Then applying the parabolic comparison to (1.1) and system (1.1) in [78] readily gives the uniform (in time) boundedness of A, A_x and ρ. Finally, one can apply the well-known Moser-iteration to obtain the uniform boundedness of u. Therefore, $T_{\max} = \infty$, and the solution is global and unique. □

Despite the nice properties in Theorem 1.1, in Section 5 we shall demonstrate that system (1.1) is not well-posed because its dynamics are not continuous to the variation of initial data.

2 Linearized stability of the constant solution

To find nontrivial spatial patterns of system (1.1), we first observe that system (1.1) always admits the following constant solution $(\bar{A}, \bar{\rho}, \bar{u})$:

$$\bar{A} := \frac{(\alpha+\beta-\bar{u}) + \sqrt{(\alpha+\beta-\bar{u})^2 + 4\alpha\bar{u}}}{2},\ \bar{\rho} := 1 - \frac{\alpha}{\bar{A}},\ \text{and}\ \bar{u} := \frac{1}{L}\int_0^L u_0(x)dx. \tag{2.1}$$

Note that both $\bar{A}$ and $\bar{\rho}$ are positive constants that depend on α, β, and $\bar{\rho} = \frac{\beta}{\bar{A}+\bar{u}}$. The purpose of this section is to determine when $(\bar{A}, \bar{\rho}, \bar{u})$ becomes unstable, leading to the formation of stable non-constant solutions and we focus on investigating the effects of policing on the criminal activity.

We linearize (1.1) about equilibrium (2.1) through the following perturbations:

$$A = \bar{A} + \epsilon\hat{A},\ \rho = \bar{\rho} + \epsilon\hat{\rho},\ \text{and}\ u = \bar{u} + \epsilon\hat{u},\ 0 < \epsilon \ll 1,$$

and collect

$$\begin{cases} \hat{A}_t \approx D_A\hat{A}_{xx} - \frac{\alpha}{\bar{A}}\hat{A} + \bar{A}\hat{\rho}, & x \in (0,L), t > 0, \\ \hat{\rho}_t \approx (D_\rho\hat{\rho}_x - 2\frac{\bar{\rho}}{\bar{A}}\hat{A}_x)_x - \bar{\rho}\hat{A} - (\bar{A}+\bar{u})\hat{\rho} - \bar{\rho}\hat{u}, & x \in (0,L), t > 0, \\ \hat{u}_t \approx (D_u\hat{u}_x - \chi\frac{\bar{u}}{\bar{A}}\hat{A}_x)_x, & x \in (0,L), t > 0, \\ \hat{A}_x(x,t) = \hat{\rho}_x(x,t) = \hat{u}_x(x,t) = 0, & x = 0, L, t > 0. \end{cases} \tag{2.2}$$

Setting the solution of (2.2) in the form $(\hat{A},\hat{\rho},\hat{u})=(C_1,C_2,C_3)e^{\sigma t+i\mathbf{kx}}$, where $\mathbf{k}$ is the wavemode vector with $|\mathbf{k}|^{\mathbf{2}}=(\frac{\mathbf{k}\pi}{\mathbf{L}})^{\mathbf{2}}$, σ is the growth rate of perturbations, and C_i are constants to be determined, we collect the following eigenvalue problem

$$\left(\sigma\mathbb{I}+\mathcal{D}|\mathbf{k}|^2+\mathcal{A}_0\right)\begin{pmatrix}C_1\\C_2\\C_3\end{pmatrix}=\begin{pmatrix}0\\0\\0\end{pmatrix},$$

where $\mathbb{I}$ is the unit matrix and matrices $\mathcal{D}$ and $\mathcal{A}_0$ are given by:

$$\mathcal{A}_0=\begin{pmatrix}-\frac{\alpha}{\bar{A}} & \bar{A} & 0\\ -\bar{\rho} & -(\bar{A}+\bar{u}) & -\bar{\rho}\\ 0 & 0 & 0\end{pmatrix}\quad\text{and}\quad\mathcal{D}=\begin{pmatrix}D_A & 0 & 0\\ -2D_\rho\frac{\bar{\rho}}{\bar{A}} & D_\rho & 0\\ -\chi D_u\frac{\bar{\rho}}{\bar{A}} & 0 & D_u\end{pmatrix}.$$

Alternatively, σ is eigenvalue of the following stability matrix associated with (1.1)

$$\mathcal{A}_k=\begin{pmatrix}-D_A(\frac{k\pi}{L})^2-\frac{\alpha}{\bar{A}} & \bar{A} & 0\\ 2\frac{\bar{\rho}}{\bar{A}}(\frac{k\pi}{L})^2-\bar{\rho} & -D_\rho(\frac{k\pi}{L})^2-(\bar{A}+\bar{u}) & -\bar{\rho}\\ \chi\frac{\bar{u}}{\bar{A}}(\frac{k\pi}{L})^2 & 0 & -D_u(\frac{k\pi}{L})^2\end{pmatrix},k\in\mathbb{N}^+,\tag{2.3}$$

and the stability of $(\bar{A},\bar{\rho},\bar{u})$ is determined by the eigenvalues of matrix (2.3).

To this end, we find the characteristic polynomial of (2.3) to be

$$\sigma^3+\alpha_2(k)\sigma^2+\alpha_1(k)\sigma+\alpha_0(\chi,k)=0,\tag{2.4}$$

with

$$\alpha_2(k):=(D_A+D_\rho+D_u)\Big(\frac{k\pi}{L}\Big)^2+(\alpha/\bar{A}+\bar{A}+\bar{u})>0,$$

$$\alpha_1(k):=(D_AD_\rho+D_AD_u+D_\rho D_u)\Big(\frac{k\pi}{L}\Big)^4+\Big[(D_u+D_A)(\bar{A}+\bar{u})+\frac{\alpha(D_u+D_\rho)}{\bar{A}}-2\bar{\rho}\Big]\Big(\frac{k\pi}{L}\Big)^2$$
$$+\alpha\Big(1+\frac{\bar{u}}{\bar{A}}\Big)+\bar{A}\bar{\rho},$$

and

$$\alpha_0(\chi,k):=\bar{\rho}\bar{u}\Big(\frac{k\pi}{L}\Big)^2(\chi-\chi_k^S),$$

where

$$\chi_k^S:=-\frac{D_u}{\bar{\rho}\bar{u}}\left\{D_AD_\rho\Big(\frac{k\pi}{L}\Big)^4+\Big[D_A(\bar{A}+\bar{u})+\frac{\alpha D_\rho}{\bar{A}}-2\bar{\rho}\Big]\Big(\frac{k\pi}{L}\Big)^2+\alpha\Big(1+\frac{\bar{u}}{\bar{A}}\Big)+\bar{A}\bar{\rho}\right\},k\in\mathbb{N}^+.\tag{2.5}$$

By the principle of the linearized stability, $(\bar{A},\bar{\rho},\bar{u})$ is asymptotically stable with respect to (1.1) if and only if all eigenvalues of the matrix (2.3) have negative real part, then according to the Routh–Hurwitz conditions, or Corollary 2.2 in [47], all roots of (2.4) are in the open left half plane of $\mathbb{C}$ if and only if α_2, $\alpha_0>0$ and $\alpha_2\alpha_1>\alpha_0$. Note that $\alpha_2(k)>0$, therefore the constant equilibrium $(\bar{A},\bar{\rho},\bar{u})$ is locally asymptotically sable with respect to (1.1) if and only if the following conditions hold for each $k\in\mathbb{N}$:

$$\alpha_0(\chi,k)>0\text{ and }\alpha_1(k)\alpha_2(k)-\alpha_0(\chi,k)>0,$$

while $(\bar{A},\bar{\rho},\bar{u})$ is unstable if one of the conditions above fails for some $k\in\mathbb{N}$. The above conditions hold for $k=0$, and we only need to examine the cases for $k\in\mathbb{N}^+$. For each $k\geq1$,

since $\alpha_2(k) > 0$, $\alpha_1(k) > 0$ if $\alpha_0(\chi, k) > 0$ and $\alpha_1(k)\alpha_2(k) - \alpha_0(\chi, k) > 0$, we have that $(\bar{A}, \bar{\rho}, \bar{u})$ is unstable if there exists any $k \in \mathbb{N}^+$ such that either $\alpha_0(\chi, k) < 0$ or $\alpha_1(k)\alpha_2(k) - \alpha_0(\chi, k) < 0$.

On the other hand, from straightforward calculations one has that

$$\alpha_0(\chi, k) < 0 \text{ if and only if } \chi < \chi_k^S \text{ for some } k \in \mathbb{N}^+$$

with χ_k^S given by (2.5) and

$$\alpha_1(k)\alpha_2(k) - \alpha_0(\chi, k) < 0 \text{ if and only if } \chi > \chi_k^H \text{ for some } k \in \mathbb{N}^+$$

with

$$\chi_k^H := \chi_k^S + \frac{\alpha_1\alpha_2}{\bar{\rho}\bar{u}(\frac{k\pi}{L})^2}, \tag{2.6}$$

therefore the constant solution $(\bar{A}, \bar{\rho}, \bar{u})$ is unstable if either

$$\chi < \max_{k\in\mathbb{N}^+} \chi_k^S \quad \text{or} \quad \chi > \min_{k\in\mathbb{N}^+} \chi_k^H,$$

otherwise, it is locally stable. The linearized stability of $(\bar{A}, \bar{\rho}, \bar{u})$ can be summarized into the following result.

Proposition 2.1. *Assume that all the parameters in (1.1) are positive, and denote*

$$\chi^- := \max_{k\in\mathbb{N}^+} \chi_k^S \quad \text{and} \quad \chi^+ := \min_{k\in\mathbb{N}^+} \chi_k^H. \tag{2.7}$$

Then the following dichotomy holds:

(i) if $\chi^- < \chi^+$, then the equilibrium $(\bar{A}, \bar{\rho}, \bar{u})$ is unstable for $\chi \in (-\infty, \chi^-) \cup (\chi^+, \infty)$ and it is locally asymptotically stable for $\chi \in (\chi^-, \chi^+)$;

(ii) if $\chi^- \geq \chi^+$, then $(\bar{A}, \bar{\rho}, \bar{u})$ is always unstable for any $\chi \in \mathbb{R}$.

It is easy to see that both χ^- and χ^+ are well-defined. For each $k \in \mathbb{N}^+$, matrix (2.3) has three (complex) eigenvalues $\sigma_i(k)$, for $i = 1, 2, 3$, each depending on χ smoothly. When $\chi = \chi_k^S$, all eigenvalues are real with $\sigma_1(k), \sigma_2(k) < 0$ and $\sigma_3(k) = 0$. On the other hand, when $\chi = \chi_k^H$, $\sigma_{1,2} = \pm i\sqrt{\alpha_1(k)}$ are coupled and purely imaginary if $\alpha_1 > 0$ and $\sigma_3 < 0$. Before concluding this section, we present the following observations that are important for our coming analysis.

Remark 2.1. *(i) if $\alpha_1(k) > 0$ for each $k \in \mathbb{N}^+$, we have from (2.6) that $\chi_k^S < \chi_k^H$. However, this does not imply $\chi^- < \chi^+$ in general, especially when diffusion rates are small. For instance, if $D_A = D_\rho = D_u = \epsilon \ll 1$, for simplicity we choose $L = \pi$ and have that*

$$\alpha_1(k) = 3\epsilon^2 k^4 + \Big(2(\bar{A} + \bar{u} + \frac{\alpha}{\bar{A}})\epsilon - 2\bar{\rho}\Big)k^2 + \alpha\Big(1 + \frac{\bar{u}}{\bar{A}}\Big) + \bar{A}\bar{\rho} \leq 3\epsilon^2 k^4 - \bar{\rho}k^2 + O(1).$$

It is easy to see that $\alpha_1(k) \approx -\frac{\bar{\rho}}{12\epsilon^2} + O(1) < 0$ when $k \approx \sqrt{\frac{\bar{\rho}}{6\epsilon}}$. Then one can easily find that $\chi_k^H < \chi_k^S$ for each $k \in \mathbb{N}^+$ hence $\chi^+ > \chi^-$. This implies that the constant solution is always unstable for any $\chi \in \mathbb{R}$. In the coming sections, we will show that its stability is lost to either a stable stationary or time-periodic solution of (1.1), depending on the system parameters;

(ii) if $\alpha_1(k_0) \leq 0$ for some $k_0 \in \mathbb{N}^+$, matrix (2.3) has at least one positive root for $\chi = \chi_{k_0}^H$, which implies the instability of $(\bar{A}, \bar{\rho}, \bar{u})$ with χ being at and around χ_H^k. Indeed, in this case, we have that $\chi_{k_0}^H \leq \chi_{k_0}^S$, therefore by definition we find that $\chi^- = \max \chi_k^S \geq \chi_{k_0}^S \geq \chi_{k_0}^H \geq \min \chi_k^H = \chi^+$, thanks to which, Proposition 2.1 implies that $(\bar{A}, \bar{\rho}, \bar{u})$ is always unstable. However, matrix (2.3) has no purely imaginary eigenvalues at $\chi = \chi_{k_0}^H$ in this case.

From the discussions above, we find that $\alpha_1(k) > 0$ is equivalent to matrix (2.3) having purely imaginary eigenvalues. Now that we are motivated to study the formation of spatially nontrivial solutions of (1.1) as the constant solution turns unstable through bifurcation theories, we will find that that time-periodic solutions bifurcate from $(\bar{A}, \bar{\rho}, \bar{u})$ at $\chi = \chi_{k_0}^H$.

3 Analysis of nonconstant positive steady states

This section is devoted to studying nonconstant positive solutions of the stationary system:

$$\begin{cases} D_A A_{xx} - A + A\rho + \alpha = 0, & x \in (0, L), \\ (D_\rho \rho_x - 2\rho A_x/A)_x - A\rho + \beta - u\rho = 0, & x \in (0, L), \\ (D_u u_x - \chi u A_x/A)_x = 0, & x \in (0, L), \\ A_x(x) = \rho_x(x) = u_x(x) = 0, & x = 0, L, \\ A, \rho, u \in C^2([0, L]), A(x), \rho(x), u(x) > 0, & x \in (0, L), \end{cases} \tag{3.1}$$

This stationary problem is important to the spatio-temporal dynamics of (1.1) since it naturally serves as one of the candidates that describe the long-time profiles of (A, ρ, u).

To find nonconstant solutions of the stationary system (3.1), we perform steady state bifurcation analysis of (3.1) at $(\bar{A}, \bar{\rho}, \bar{u})$. Now that this trivial solution becomes unstable when χ escapes the interval (χ^-, χ^+) according to Proposition 2.1, we are concerned with the conditions when spatially inhomogeneous solutions can emerge. Before presenting further analysis, we point out that the maximum principle implies that A has a uniform positive lower bound. Though our analysis carries over to the case when $\alpha = 0$, we record this fact here for future reference.

3.1 Existence of nonconstant positive steady states

To investigate the effects of policing strength on the formation and qualitative dynamics of nontrivial patterns throughout (3.1), we treat χ as the bifurcation parameter, introduce the following function spaces

$$\mathcal{X} = \{w \in H^2((0, L)) | w_x(0) = w_x(L) = 0\} \text{ and } \mathcal{Y} = L^2((0, L))$$

and then convert (3.1) into the following abstract form

$$\mathcal{F}(A, \rho, u, \chi) = 0 \text{ for } (A, \rho, u, \chi) \in \mathcal{X}^3 \times \mathbb{R},$$

where $\mathcal{X}^3 = \mathcal{X} \times \mathcal{X} \times \mathcal{X}$ and

$$\mathcal{F}(A, \rho, u, \chi) = \begin{pmatrix} D_A A_{xx} - A + A\rho + \alpha \\ (D_\rho \rho_x - 2\rho A_x/A)_x - A\rho + \beta - u\rho \\ (D_u u_x - \chi u A_x/A)_x \end{pmatrix}. \tag{3.2}$$

The problem of finding solutions of (3.1) turns into finding nontrivial positive roots of $\mathcal{F}$ in $\mathcal{X}^3 \times \mathbb{R}$. One can then apply the standard elliptic regularity theory to find that these roots are classical solutions.

To this end, we first observe that $\mathcal{F}(\bar{A}, \bar{\rho}, \bar{u}, \chi) = 0$ for any $\chi \in \mathbb{R}$ and $\mathcal{F} : \mathcal{X}^3 \times \mathbb{R} \to \mathcal{Y}^3$ is analytic. Moreover, for any fixed $(A^*, \rho^*, u^*) \in \mathcal{X}^3$, the Fréchet derivative of $\mathcal{F}$ is given by

$$D\mathcal{F}_{(A,\rho,u)}(A^*, \rho^*, u^*, \chi) = \begin{pmatrix} D_A A_{xx} + (\rho^* - 1)A + A^*\rho \\ D_\rho \rho_{xx} - 2\big[\big(\frac{\rho}{A^*} - \frac{\rho^* A}{(A^*)^2}\big)A^*{}_x + \frac{\rho^*}{A^*}A_x\big]_x - \rho^*(A + u) - (A^* + u^*)\rho \\ D_u u_{xx} - \chi\big[\big(\frac{u}{A^*} - \frac{u^* A}{(A^*)^2}\big)A^*{}_x + \frac{u^*}{A^*}A_x\big]_x \end{pmatrix}. \tag{3.3}$$

Below, we collect another important fact about $\mathcal{F}$.

Lemma 3.1. *$D\mathcal{F}_{(A,\rho,u)}(A^*, \rho^*, u^*, \chi) : \mathcal{X}^3 \times \mathbb{R} \to \mathcal{Y}^3$ is a Fredholm operator with zero index.*

Proof. We denote $\mathbf{u}=(A,\rho,u)^T$ and rewrite (3.3) as

$$D\mathcal{F}_{(A,\rho,u)}(A^*,\rho^*,u^*,\chi)=\mathcal{A}_0(\mathbf{u})\mathbf{u}_{xx}+\mathbf{F}_0(x,\mathbf{u},\mathbf{u}_x),$$

where

$$\mathcal{A}_0=\begin{pmatrix} D_A & 0 & 0\\ -2\frac{\rho^*}{A^*} & D_\rho & 0\\ -\chi\frac{u^*}{A^*} & 0 & D_u\end{pmatrix},\mathbf{F}_0(x,\mathbf{u},\mathbf{u}_x)=\begin{pmatrix} (\rho^*-1)A+A^*\rho\\ -2\big[(\frac{\rho}{A^*}-\frac{\rho^*A}{(A^*)^2})A^*{}_x\big]_x-\rho^*(A+u)-(A^*+u^*)\rho\\ -\chi\big[(\frac{u}{A^*}-\frac{u^*A}{(A^*)^2})A^*{}_x\big]_x\end{pmatrix}.$$

Here operator (3.3) is elliptic since all eigenvalues of $\mathcal{A}_0$ are positive. According to Remark 2.5 (case 2) in [66] with $N=1$, $\mathcal{A}_0$ satisfies the Agmon's condition (see Definition 2.4 in [66]). Therefore, $D\mathcal{F}_{(A,\rho,u)}(A^*,\rho^*,u^*,\chi)$ is Fredholm with zero index due to Theorem 3.3 and Remark 3.4 of [66]. **Λ**

To seek spatially non-trivial solutions of (3.1) that bifurcate from the equilibrium $(\bar{A},\bar{\rho},\bar{u})$, we first check the following necessary condition

$$\mathcal{N}(D\mathcal{F}(\bar{A},\bar{\rho},\bar{u},\chi))\neq\{\mathbf{0}\},\tag{3.4}$$

where operator $D\mathcal{F}$ is given by (3.3) and $\mathcal{N}$ denotes its null space in $\mathcal{X}^3$. For this purpose, we choose $(A^*,\rho^*,u^*)=(\bar{A},\bar{\rho},\bar{u})$ in (3.2) and find that the null space in (3.4) consists of solution (A,ρ,u) of the following problem

$$\begin{cases} D_AA_{xx}+(\bar{\rho}-1)A+\bar{A}\rho=0, & x\in(0,L),\\ D_\rho\rho_{xx}-\frac{2\bar{\rho}}{\bar{A}}A_{xx}-\bar{\rho}(A+u)-(\bar{A}+\bar{u})u=0, & x\in(0,L),\\ D_uu_{xx}-\chi\frac{\bar{u}}{\bar{A}}A_{xx}=0, & x\in(0,L),\\ A_x(x)=\rho_x(x)=u_x(x)=0, & x=0,L.\end{cases}\tag{3.5}$$

In light of the following eigen-expansions

$$A(x)=\sum_{k=0}^{\infty}t_k\cos\left(\frac{k\pi x}{L}\right),\rho(x)=\sum_{k=0}^{\infty}s_k\cos\left(\frac{k\pi x}{L}\right),u(x)=\sum_{k=0}^{\infty}r_k\cos\left(\frac{k\pi x}{L}\right)$$

with t_k, s_k and r_k being constants, we have that

$$\begin{pmatrix} -D_A(\frac{k\pi}{L})^2-\alpha/\bar{A} & \bar{A} & 0\\ 2\frac{\bar{\rho}}{\bar{A}}(\frac{k\pi}{L})^2 & -D_\rho(\frac{k\pi}{L})^2-(\bar{A}+\bar{u}) & -\bar{\rho}\\ \chi\frac{\bar{u}}{\bar{A}}(\frac{k\pi}{L})^2 & 0 & -D_u(\frac{k\pi}{L})^2\end{pmatrix}\begin{pmatrix}t_k\\ s_k\\ r_k\end{pmatrix}=\begin{pmatrix}0\\0\\0\end{pmatrix}\text{ for }k\in\mathbb{N}^+.\tag{3.6}$$

Note that $k=0$ is ruled out as it gives rise to the constant solution $(\bar{A},\bar{\rho},\bar{u})$, whereas we look for spatially nonconstant solutions. For each $k\in\mathbb{N}^+$, (3.5) has nonzero solutions if and only if the coefficient matrix of (3.6) is singular or equivalently $\chi=\chi_k^S$ given by (2.4) for some k.

Once condition (3.4) is satisfied at $\chi=\chi_k^S$, we easily find that $\mathcal{N}(D\mathcal{F}(\bar{A},\bar{\rho},\bar{u},\chi))=\text{span}\{(\bar{A}_k,\bar{\rho}_k,\bar{u}_k)\}$, and it is one-dimensional

$$\bar{A}_k=P_k\cos\left(\frac{k\pi x}{L}\right),\bar{\rho}_k=Q_k\cos\left(\frac{k\pi x}{L}\right),\bar{u}_k=\cos\left(\frac{k\pi x}{L}\right),\tag{3.7}$$

where

$$P_k:=\frac{D_u\bar{A}}{\chi_k\bar{u}},Q_k:=\frac{D_u(D_A(\frac{k\pi}{L})^2+\alpha/\bar{A})}{\chi_k\bar{u}},k\in\mathbb{N}^+.\tag{3.8}$$

Having the potential bifurcation values χ_k^S in (2.5), we now prove in the following theorem that the steady state bifurcation occurs at $(\bar{A},\bar{\rho},\bar{u},\chi_k)$ for each $k\in\mathbb{N}^+$, which establishes the existence of nonconstant positive solutions of (3.1).

Theorem 3.2. *Suppose that $\chi_k^S \neq \chi_j^S, \forall k \neq j$, χ_k^S given by (2.5) and (2.6) respectively. Then for each $k \in \mathbb{N}^+$, there exist a positive constant δ and a unique one-parameter curve $\Gamma_k(s) = \{(A_k(s,x), \rho_k(s,x), u_k(s,x), \chi_k(s)) : s \in (-\delta, \delta)\}$ of spatially inhomogeneous solutions $(A, \rho, u, \chi) \in \mathcal{X}^3 \times \mathbb{R}$ to (3.1) that bifurcate from $(\bar{A}, \bar{\rho}, \bar{u})$ at $\chi = \chi_k^S$. Moreover, each function is smooth in s and*

$$(A_k(s,x), \rho_k(s,x), u_k(s,x)) = (\bar{A}, \bar{\rho}, \bar{u}) + s(\bar{A}_k, \bar{\rho}_k, \bar{u}_k) + \boldsymbol{O}(s^2), s \in (-\delta, \delta), \tag{3.9}$$

and

$$\chi_k(s) = \chi_k^S + O(s), s \in (-\delta, \delta), \tag{3.10}$$

where $(\bar{A}_k, \bar{\rho}_k, \bar{u}_k)$ is given by (3.7)-(3.8), and $\boldsymbol{O}(s^2) \in \mathcal{Z}$ is in the closed complement of $\mathcal{N}(D\mathcal{F}(\bar{A}, \bar{\rho}, \bar{u}, \chi))$ defined by

$$\mathcal{Z} = \Big\{(A, \rho, u) \in \mathcal{X}^3 \Big| \int_0^L A\bar{A}_k + \rho\bar{\rho}_k + u\bar{u}_k dx = 0\Big\}. \tag{3.11}$$

Proof. We have verified all the necessary conditions except the following to apply the Crandall–Rabinowitz local theory in [20]

$$\frac{d}{d\chi}(D\mathcal{F}(\bar{A}, \bar{\rho}, \bar{u}, \chi))(\bar{A}_k, \bar{\rho}_k, \bar{u}_k)|_{\chi=\chi_k^S} \notin \mathcal{R}(D\mathcal{F}(\bar{A}, \bar{\rho}, \bar{u}, \chi)), \tag{3.12}$$

where $\mathcal{R}$ is the range of the operator. We argue by contradiction and suppose that condition (3.12) fails. Then, there exists a nontrivial solution (A, ρ, u) that satisfies

$$\begin{cases} D_A A_{xx} + (\bar{\rho} - 1)A + \bar{A}\rho = 0, & x \in (0, L), \\ D_\rho \rho_{xx} - \frac{2\bar{\rho}}{\bar{A}} A_{xx} - \bar{\rho}(A + u) - (\bar{A} + \bar{u})u = 0, & x \in (0, L), \\ D_u u_{xx} - \chi \frac{\bar{u}}{\bar{A}} A_{xx} = -\frac{\bar{u}}{\bar{A}}(A_k)_{xx} = \frac{\bar{u}}{\bar{A}}\left(\frac{k\pi}{L}\right)^2 P_k, & x \in (0, L), \\ A_x(x) = \rho_x(x) = u_x(x) = 0, & x = 0, L. \end{cases} \tag{3.13}$$

Multiplying equations in (3.13) by $\cos\left(\frac{k\pi x}{L}\right)$ and integrating them over $(0, L)$ by parts, we obtain that

$$\begin{pmatrix} -D_A(\frac{k\pi}{L})^2 - \alpha/\bar{A} & \bar{A} & 0 \\ 2\frac{\bar{\rho}}{\bar{A}}(\frac{k\pi}{L})^2 & -D_\rho(\frac{k\pi}{L})^2 - (\bar{A} + \bar{u}) & -\bar{\rho} \\ \chi\frac{\bar{u}}{\bar{A}}(\frac{k\pi}{L})^2 & 0 & -D_u(\frac{k\pi}{L})^2 \end{pmatrix} \begin{pmatrix} \int_0^L A\cos\frac{k\pi x}{L} dx \\ \int_0^L \rho\cos\frac{k\pi x}{L} dx \\ \int_0^L u\cos\frac{k\pi x}{L} dx \end{pmatrix} = \begin{pmatrix} 0 \\ 0 \\ \frac{(k\pi)^2\bar{u}}{2\bar{A}L} \end{pmatrix}.$$

However, the coefficient matrix is singular thanks to (2.5) which implies that this system has no solution for each $k \in \mathbb{N}^+$, then we reach a contradiction and this completes the proof of condition (3.12). Then the statements in Theorem 3.2 follow from Theorem 1.7 of [20]. **Λ**

3.2 Stability of nonconstant positive steady states

A natural question concerning the stability of the spatially inhomogeneous bifurcating solution $(A_k(s,x), \rho_k(s,x), u_k(s,x))$ established in Theorem 3.2 arises. Here the stability or instability is that of the bifurcating solution regarded as an equilibrium of system (3.1). To this end, we want to determine the turning direction of the bifurcation branch $\Gamma_k(s)$ around each bifurcation point. It is easy to see that the operator $\mathcal{F}$ is C^4-smooth, and according to Theorem 1.18 in [21] we can write the following expansions

$$\begin{cases} A_k(s,x) = \bar{A} + sP_k\cos\left(\frac{k\pi x}{L}\right) + s^2\varphi_1(x) + s^3\varphi_2(x) + o(s^3), \\ \rho_k(s,x) = \bar{\rho} + sQ_k\cos\left(\frac{k\pi x}{L}\right) + s^2\psi_1(x) + s^3\psi_2(x) + o(s^3), \\ u_k(s,x) = \bar{u} + s\cos\left(\frac{k\pi x}{L}\right) + s^2\gamma_1(x) + s^3\gamma_2(x) + o(s^3), \\ \chi_k(s) = \chi_k^S + s\mathcal{K}_1 + s^2\mathcal{K}_2 + o(s^2), \end{cases} \tag{3.14}$$

where $(\phi_i, \psi_i, \gamma_i) \in \mathcal{Z}$ in (3.11) and $\mathcal{K}_i$ are constants for $i = 1, 2$. $o(s^3)$ are taken with respect to the $\mathcal{X}$-topology and $o(s^2)$ is a real number.

One can easily show that each bifurcation branch $\Gamma_k(s)$ is of pitch-fork, *i.e.* being one sided. Now we give stability of the bifurcating solutions in terms of the sign of $\mathcal{K}_2$.

Theorem 3.3. *Suppose that all the conditions in Theorem 3.2 are satisfied and let* $\Gamma_k(s) = \{(A_k(s,k), \rho_k(s,k), u_k(s,k), \chi_k(s))\}$ *be the* k^{th} *bifurcation branch given by (3.9)-(3.10). Denote* $\chi_0 = \min_{k\in\mathbb{N}^+}\{\chi_k^S, \chi_k^H\}$ *as in (2.7). Then the followings hold:*

(i) if $\chi_0 = \chi_{k_0}^S < \min_{k\in\mathbb{N}^+}\chi_k^H$, *then* $\Gamma_{k_0}(s)$ *around* $(\bar{A}, \bar{\rho}, \bar{u}, \chi_{k_0})$ *is asymptotically stable for* $\mathcal{K}_2 > 0$ *and it is unstable for* $\mathcal{K}_2 < 0$, *while* $\Gamma_k(s)$ *around* $(\bar{A}, \bar{\rho}, \bar{u}, \chi_k)$ *is always unstable for each* $k \neq k_0$;

(ii) if $\chi_0 = \chi_{k_1}^H < \min_{k\in\mathbb{N}^+}\chi_k^S$, *then* $\Gamma_k(s)$ *around* $(\bar{A}, \bar{\rho}, \bar{u}, \chi_k)$ *is always unstable for each* $k \in \mathbb{N}^+$.

Remark 3.1. *Our results suggest that* $(\bar{A}, \bar{\rho}, \bar{u}, \chi_k^S)$ *looses its stability to the stable steady state bifurcating solution with wavemode number* k_0 *for which* χ_k^S *achieves its minimum over* $\mathbb{N}^+$. *When case (ii) occurs, we prove in section 4 that stability is lost to stable Hopf bifurcating solutions. This is numerically illustrated in Section 5.*

Proof of Theorem 3.3. Our proof follows the approaches in [76, 80] based on slight modifications in the arguments for Corollary 1.13 of [21], or Theorem 3.2 of [76], Theorem 5.5, Theorem 5.6 of [18]. We shall only prove case (ii) and case (i) can be proved very similarly.

For each $k \in \mathbb{N}^+$, we linearize (1.1) around $(A_k(s,x), \rho_k(s,x), u_k(s,x), \chi_k(s))$ and obtain the following eigenvalue problem

$$D\mathcal{F}(A_k(s,x), \rho_k(s,x), u_k(s,x), \chi_k(s))(A,\rho,u) = \sigma(s)(A,\rho,u),\ (A,\rho,u) \in \mathcal{X}\times\mathcal{X}\times\mathcal{X},$$

then $(A_k(s,x), \rho_k(s,x), u_k(s,x), \chi_k(s))$ is asymptotically stable if and only if the real part of eigenvalue $\sigma(s)$ is negative.

Sending $s \to 0$ in (3.14), we know from the verification for (3.12) that $\bar{\sigma} = 0$ is a simple eigenvalue of $D\mathcal{F}(\bar{A}, \bar{\rho}, \bar{u}, \chi_k^S) = \sigma(A, \rho, u)$ or equivalently the following problem

$$\begin{cases} D_A A'' - \alpha_1 \bar{A} A + \bar{A}\rho = \sigma A, & x \in (0, L), \\ D_\rho \rho'' - 2\frac{\bar{\rho}}{\bar{A}} A'' - (\bar{A} + \bar{u})\rho - \bar{\rho} u = \sigma\rho, & x \in (0, L), \\ D_u u'' - 2\chi_k^S \frac{\bar{\rho}}{\bar{A}} A'' = \sigma u, & x \in (0, L). \\ A'(x) = \rho'(x) = u'(x) = 0, & x = 0, L, \end{cases}$$

the eigen-space of which is one-dimensional and $\mathcal{N}\big(D\mathcal{F}(\bar{A}, \bar{\rho}, \bar{u}, \chi_k^S)\big) = \{(P_k, Q_k, 1)\cos\frac{k\pi x}{L}\}$, which is not in the range of $\mathcal{R}\big(D\mathcal{F}(\bar{A}, \bar{\rho}, \bar{u}, \chi_k^S)\big)$. Multiplying the system above by $\cos\frac{k\pi x}{L}$ and integrating them over $(0, L)$ by parts, we have that $\sigma = 0$ is an eigenvalue of (2.3) with $\chi = \chi_k^S$ which reads

$$\begin{pmatrix} -D_A(\frac{k\pi}{L})^2 - \alpha_1\bar{A} & \bar{A} & 0 \\ 2\frac{\bar{\rho}}{\bar{A}}(\frac{k\pi}{L})^2 & -D_\rho(\frac{k\pi}{L})^2 - (\bar{A}+\bar{u}) & -\bar{\rho} \\ \chi_k^S\frac{\bar{u}}{\bar{A}}(\frac{k\pi}{L})^2 & 0 & -D_u(\frac{k\pi}{L})^2 \end{pmatrix}.$$

If $\chi_0 = \min_{k\in\mathbb{N}^+}\chi_k^H < \chi_k^S$ for all $k \in \mathbb{N}^+$, or $\chi_0 = \min_{k\in\mathbb{N}^+}\chi_k^S < \chi_k^H$ for $k \neq k_0$, we have from the proof of Proposition 2.1 that this matrix has at least one eigenvalue σ with positive real part. From the standard eigenvalue perturbation theory in [42], an eigenvalue $\sigma(s)$ to the linearized problem above that has a positive real part for s small. Therefore, $(A_k(s,x), \rho_k(s,x), u_k(s,x), \chi_k(s))$ is unstable for $s \in (-\delta, \delta)$. **Λ**

Theorem 3.3 implies that the only stable bifurcation branch must be $\Gamma_{k_0}(s)$ that $\chi_{k_0} = \min_{k\in\mathbb{N}^+}\{\chi_k^S, \chi_k^H\}$, and $(\bar{A}, \bar{\rho}, \bar{u})$ loses its stability only to nonconstant steady state with a spatial profile of the form $\cos\left(\frac{k_0\pi x}{L}\right)$. This gives a wavemode selection mechanism for system (1.1) when χ is around the bifurcation value. In general, it is very difficult to determine whether χ_0 is achieved at χ_k^S or χ_k^H. According to the discussions after Remark 2.1, if the interval length L is sufficiently small, $\chi_0 = \chi_1^S < \min_{k\in\mathbb{N}^+}\chi_k^H$ and the only stable bifurcating solution has wavemode $\cos\frac{\pi x}{L}$ which is spatially monotone. The wavemode section mechanism given in Theorem 3.3 is verified and illustrated in our numerical studies of (1.1) in the Section 5.

4 Hopf bifurcation and stability of periodic patterns

In this section, we study time-periodic orbits of (3.1) that bifurcate from $(\bar{A}, \bar{\rho}, \bar{u})$ at $\chi = \chi_k^H$. We want to show that if the minimum is achieved at $\chi_{k_0}^H$ for some k_0, then the constant equilibrium $(\bar{A}, \bar{\rho}, \bar{u})$ loses its stability through a Hopf bifurcation as χ surpasses $\chi_0 = \min_{k\in\mathbb{N}^+}\chi_k^H$. To apply the bifurcation theory for (3.1) at point $\chi = \chi_k^H$, we must first verify that the real part of eigenvalue crosses the imaginary axis at χ_k^H.

Discussions above imply that a Hopf bifurcation occurs at $(\bar{A}, \bar{\rho}, \bar{u})$ only if $\chi = \chi_k^H$, for which the stability matrix (2.3) has purely imaginary eigenvalues given by:

$$\sigma_1^H(\chi_k^H, k) = -\alpha_2(k) < 0, \sigma_{2,3}^H(\chi_k^H, k) = \pm i\sqrt{\alpha_1(k)}.$$

Moreover, according to Section 3, the stability matrix (2.3) has a pair of purely imaginary eigenvalues if and only if $\chi = \chi_k^H < \chi_k^S$. Therefore, a Hopf bifurcation may occur at $(\bar{A}, \bar{\rho}, \bar{u}, \chi_k^H)$ only when $\chi_k^H < \chi_k^S$. We shall always assume this condition in the coming Hopf bifurcation analysis.

4.1 Existence of time-periodic patterns

In this subsection, we prove the existence of a Hopf bifurcation. Our main result on the existence of nontrivial periodic orbits of parabolic system (3.1) states as follows.

Theorem 4.1. *Suppose that all parameters in (3.1) are positive and $\chi_k^H \neq \chi_j^H$ for $\forall j \neq k$ and $\chi_k^H < \chi_k^S$, then there exist a positive constant δ and a unique one-parameter family of nontrivial periodic orbits $\vartheta_k(s) = (\boldsymbol{u}_k(s,x,t), T_k(s), \chi_k(s)), s \in (-\delta,\delta) \to C^3(\mathbb{R}, \mathcal{X}^3) \times \mathbb{R}^+ \times \mathbb{R}$ with*

$$\boldsymbol{u}_k(s,x,t) = (\bar{A}, \bar{\rho}, \bar{u}) + s(V_k^+ e^{i\tau_0 t} + V_k^- e^{-i\tau_0 t})\cos\left(\frac{k\pi x}{L}\right) + o(s) \tag{4.1}$$

such that $(\boldsymbol{u}_k(s,x,t), \chi_k(s))$ is a nontrivial solution of (3.1) and $\boldsymbol{u}_k(s,x,t)$ is periodic of time t with period $T_k(s) \approx \frac{2\pi}{\tau_0}, \tau_0 = \sqrt{\alpha_1(k)}$, and $\{(V_k^{\pm}, \pm i\tau_0)\}$ are eigen-pairs of matrix (2.3). Moreover, $\vartheta_k(s_1) \neq \vartheta_k(s_2)$ for all $s_1 \neq s_2 \in (-\delta,\delta)$ and all nontrivial periodic solutions around $(\bar{A}, \bar{\rho}, \bar{u}, \chi_k^H)$ must be on the orbit $\vartheta_k(s), s \in (-\delta,\delta)$. In other words, if (3.1) has a nontrivial periodic solution $\boldsymbol{u}_1(x,t)$ with period T for some $\chi \in \mathbb{R}$ around $\vartheta_k(s)$ and a small positive constant ϵ such that $|\chi - \chi_k^H(s)| < \epsilon, |T - \frac{2\pi}{\tau_0}| < \epsilon$ and $\max_{t\in\mathbb{R}^+, x\in\bar{\Omega}}|\boldsymbol{u}_1(x,t) - (\bar{A}, \bar{\rho}, \bar{u})| < \epsilon$, then there exist constants $s_0 \in (-\delta,\delta)$ and $\theta_0 \in [0, 2\pi)$ such that $(T, \chi) = (T_k(s_0), \chi_k^H(s_0))$ and $\boldsymbol{u}_1(x,t) = \boldsymbol{u}_k(s_0, x, t+\theta_0)$.

Proof. We follow the proof of Theorem 5.2 in [79]. According to Proposition 2.1 and Remark 2.1, the stability matrix (2.3) with $\chi = \chi_k^H$ has a pair of purely imaginary eigenvalues $\sigma_{2,3}^H(k) = \pm\sqrt{\alpha_1(\chi_k^H)}i$; moreover since $\chi_k^H \neq \chi_j^H$ for $\forall j \neq k$, matrix (2.3) has no eigenvalue of the form $m\tau_0 i$ for $m \in \mathbb{N}^+\backslash\{\pm 1\}$.

Let $\sigma_1^H(\chi,k)$ and $\sigma_{2,3}^H(\chi,k) = \lambda(\chi,k) \pm i\tau(\chi,k)$ be the unique eigenvalues of (2.3) in a neighbourhood of $\chi = \chi_k^H$. Then σ_1^H, λ and τ are real and analytical functions of χ such that $\lambda(\chi_k^H,k) = 0$ and $\tau(\chi_k^H,k) = \tau_0 > 0$. To apply Hopf bifurcation theory, we need to prove the following transversality condition

$$\frac{\partial \lambda(\chi,k)}{\partial \chi}\Big|_{\chi=\chi_k^H} \neq 0. \tag{4.2}$$

Substitute the eigenvalues $\sigma_1^H(\chi,k)$ and $\sigma_{2,3}^H(\chi,k) = \lambda(\chi,k) \pm i\tau(\chi,k)$ into the characteristic polynomial and equate the real and imaginary parts there, then we have

$$\begin{cases} -\alpha_2(k) & = 2\lambda(\chi,k) + \sigma_1^H(\chi,k), \\ \alpha_1(k) & = \lambda^2(\chi,k) + \tau^2(\chi,k) + 2\lambda(\chi,k)\sigma_1^H(\chi,k), \\ -\alpha_0(\chi,k) & = (\lambda^2(\chi,k) + \tau^2(\chi,k))\sigma_1^H(\chi,k). \end{cases} \tag{4.3}$$

As α_1 and α_2 are independent of χ, differentiating (4.3) with respect to χ gives us

$$\begin{cases} 2\lambda' + (\sigma_1^H)' & = 0, \\ 2\lambda\lambda' + 2\tau\tau' + 2\lambda'\sigma_1^H + 2\lambda(\sigma_1^H)' & = 0, \\ (2\lambda\lambda' + 2\tau\tau')\sigma_1^H + (\lambda^2+\tau^2)(\sigma_1^H)' & = -\alpha_0' = D_u\big(\frac{k\pi}{L}\big)^2\bar{\rho}\bar{u}, \end{cases} \tag{4.4}$$

where $' = \frac{d}{d\chi}$ and we have skipped (χ,k) in each function for simplicity of notation.

Since $\lambda(\chi_k^H,k) = 0$ and $\sigma_1(\chi_k^H,k) = -\alpha_2(k)$, the last two equations in (4.4) at $\chi = \chi_k^H$ imply

$$(\sigma_1^H)'|_{\chi=\chi_k^H} = \frac{D_u\big(\frac{k\pi}{L}\big)^2\bar{\rho}\bar{u}}{\tau^2 + (\sigma_1^H)^2}\Big|_{\chi=\chi_k^H} > 0,$$

and then the first equation there easily implies $\lambda'(\chi_k^H,k) = -\frac{1}{2}(\sigma_1^H)'|_{\chi=\chi_k^H} < 0$. This verifies (4.2), and Theorem 4.1 follows from Theorem 1 in [1]. **Λ**

Theorem 4.1 implies that system (3.1) admits time-periodic spatial patterns that bifurcate from $(\bar{A},\bar{\rho},\bar{u},\chi_k^H)$ if and only if $\chi_k^H < \chi_k^S$. Furthermore, it gives the explicit expression of the time periodic spatial patterns as ϑ_k mentioned above, which admits spatial profile of the eigenfunction $\cos\big(\frac{k\pi x}{L}\big)$.

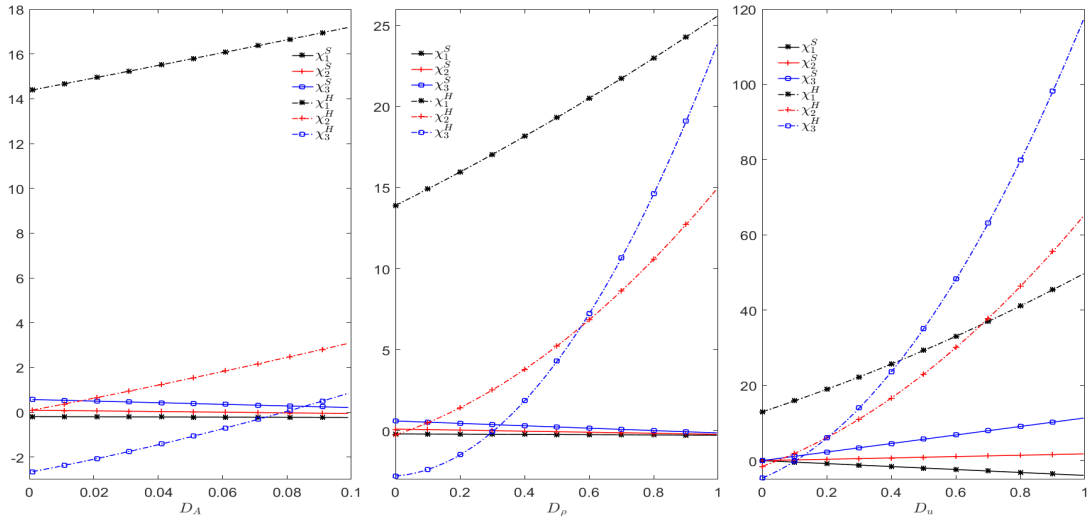

Figure 1: Bifurcation values χ_k^H and χ_k^S for various diffusion rates with $L = \pi$ and $\alpha = \beta = 1$. We set $D_\rho = D_u = 0.05$ on the left, $D_A = 0.001, D_u = 0.05$ in the center, $D_A = 0.001, D_\rho = 0.05$ on the right, and vary D_A, D_ρ and D_u, respectively. These graphs tend to suggest that increasing diffusion rate can lead to larger values of χ_k^H, hence promoting the emergence of periodic patterns.

As discussed above, it is difficult to determine the necessary condition for $\chi_k^H < \chi_k^S$ in terms of system parameters. Figure 1 presents three plots demonstrating the variation of bifurcation values against the diffusion rates. All plots indicate that increasing diffusion rate gives rise to larger χ_k^H and helps promote the emergence of periodic patterns according to our discussions.

However, if the interval L is sufficiently small, it always holds that $\chi_k^H > \chi_k^S$ for each $k \in \mathbb{N}^+$. This indicates that Hopf bifurcations do not occur for small interval lengths. Indeed, from the discussions after the proof of Theorem 3.3 we know that, in this case, the stability of the homogeneous solution $(\bar{A}, \bar{\rho}, \bar{u})$ is lost through the first bifurcation branch $(\bar{A}, \bar{\rho}, \bar{u}, \chi_1^S)$, which has stable stationary solution of (3.1) with eigenfunction $\cos\left(\frac{\pi x}{L}\right)$.

4.2 Stability of time-periodic patterns

Next, we study the stability of the time-periodic solutions obtained in Theorem 4.1. Again, by stability here we mean the formal linearized stability of a periodic solution relative to perturbations from $\vartheta_k(s)$. Suppose that $\chi_{k_0}^H = \min_{k\in\mathbb{N}^+} \chi_k^H < \chi_k^S, \forall k \in \mathbb{N}^+$, and assume that all the conditions in Theorem 4.1 are satisfied, then our stability results show that $\vartheta_k(s)$, $s \in (-\delta, \delta)$ is asymptotically stable only if $\chi = \chi_{k_0}^H$.

Denote $\mathbf{u}_k(s,x,t) = (A_k(s,x,t), \rho_k(s,x,t), u_k(s,x,t))$ and let $(\mathbf{u}_k(s,x,t), T_k(s), \chi_k(s))$ be the periodic solutions on the branch $\vartheta_k(s)$ obtained in Theorem 4.1. Rewrite (3.1) as

$$\frac{d\mathbf{u}_k}{dt} = g(\mathbf{u}_k, \chi_k(s)), t > 0$$

with

$$g(\mathbf{u}_k, \chi_k(s)) = \begin{pmatrix} D_A A_{xx} - A + A\rho + \alpha \\ (D_\rho \rho_x - 2\rho A_x/A)_x - (A+u)\rho + \beta \\ (D_u u_x - \chi_k(s) u A_x/A)_x \end{pmatrix},$$

where we skip the index k. Differentiating (3.1) against t, with $\tilde{\mathbf{u}}_k = \frac{du}{dt}$ we have that

$$\frac{d\tilde{\mathbf{u}}_k}{dt} = g_{\mathbf{u}}(\mathbf{u}_k, \chi_k(s))\tilde{\mathbf{u}}_k,$$

then we observe that zero is a Floquet exponent and one is a Floquet multiplier for $\mathbf{u}_k$.

Linearize the periodic solution around the bifurcation branch $\vartheta_k(s)$ by substituting the perturbed solution $\mathbf{u}_k + \mathbf{w}e^{-lt}$, where $\mathbf{w}$ is a sufficiently small T-periodic function and $l = l(s)$ is a continuous function of s, then we have that

$$\frac{d\mathbf{w}(s,t)}{dt} = g_{\mathbf{u}}(\mathbf{u}_k, \chi_k(s))\mathbf{w}(s,t) + k(s)\mathbf{w}(s,t) \tag{4.5}$$

where $g_{\mathbf{u}}$ is the Fréchet derivative with respect to $\mathbf{u}$ and it is explicitly given by

$$g_{\mathbf{u}}(\mathbf{u}_k, \chi_k(s)) = \begin{pmatrix} D_A A_{xx} + (\rho_k - 1)A + A_k\rho \\ D_\rho \rho_{xx} - 2\left[\left(\frac{\rho}{A_k} - \frac{\rho_k A}{A_k^2}\right)(A_k)_x + \frac{\rho_k}{A_k}A_x\right]_x - \rho_k(A+u) - (A_k + u_k)\rho \\ D_u u_{xx} - \chi_k(s)\left[\left(\frac{u}{A_k} - \frac{u_k A}{A_k^2}\right)(A_k)_x + \frac{u_k}{A_k}A_x\right]_x \end{pmatrix}.$$

The stability of the bifurcating solutions around χ_k^H can be determined by computing the eigenvalues of this reduced equation. When $s = 0$, (4.5) is associated with the eigenvalue problem

$$g_0(k)\mathbf{w} = k(0)\mathbf{w},$$

where

$$g_0(k) = \begin{pmatrix} D_A\frac{d^2}{dx^2} - \alpha/\bar{A} & \bar{A} & 0 \\ -2\frac{\bar{\rho}}{\bar{A}}\frac{d^2}{dx^2} & D_\rho\frac{d^2}{dx^2} - (\bar{A}+\bar{u}) & -\bar{\rho} \\ -\chi_k^H\frac{\bar{u}}{\bar{A}}\frac{d^2}{dx^2} & 0 & D_u\frac{d^2}{dx^2} \end{pmatrix},$$

and its spectrum is of infinite dimension. Note that g_0 corresponds to the matrix

$$\mathcal{A}_j(\chi_k^H) = \begin{pmatrix} -D_A(\frac{j\pi}{L})^2 - \alpha/\bar{A} & \bar{A} & 0 \\ 2\frac{\bar{\rho}}{\bar{A}}(\frac{j\pi}{L})^2 & -D_\rho(\frac{j\pi}{L})^2 - (\bar{A}+\bar{u}) & -\bar{\rho} \\ \chi_k^H\frac{\bar{u}}{\bar{A}}(\frac{j\pi}{L})^2 & 0 & -D_u(\frac{j\pi}{L})^2 \end{pmatrix} \text{ for } j \in \mathbb{N}^+. \tag{4.6}$$

Suppose that $\min_{k\in\mathbb{N}^+}\{\chi_k^H, \chi_k^S\} = \chi_{k_0}^H$ for some $k_0 \in \mathbb{N}^+$. We first show that $\vartheta_k(s)$ around χ_k^H is unstable for any $k \neq k_0$. Denote the eigenvalues of $\mathcal{A}_k(\chi_k^H)$ by $\sigma_1^H(\chi_k^H, k)$, $\sigma_2^H(\chi_k^H, k)$ and $\sigma_3^H(\chi_k^H, k)$. According to the Proposition 2.1, there exists at least one eigenvalue with positive real part if $\chi > \chi_0$. Therefore, for any positive integer $k \neq k_0$, we have that $g_0(k)$ must have an eigenvalue with positive real part hence $l(0) < 0$ if $k \neq k_0$. By the standard perturbation theory for an eigenvalue of finite multiplicity [34, 42], $l(s) < 0$ for s being small if $k \neq k_0$, and all the bifurcation branches $\vartheta_k(s)$ around $(\bar{A}, \bar{\rho}, \bar{u})$ are unstable if $k \neq k_0$. That being said, if a periodic bifurcation solution is stable, it must be on the $\vartheta_{k_0}(s)$ branch where $\chi_{k_0}^H < \min_{k\in\mathbb{N}^+}\chi_k^S$, i.e., it is on the left-most branch, while the branches on its right hand side are always unstable.

To show the stability of branch $\vartheta_{k_0}(s)$ around $(\bar{A}, \bar{\rho}, \bar{u}, \chi_{k_0}^H)$, we note from Lemma 2.10 in [22] that, the eigenvalue $l(k)$ is a continuous function real function of s near the origin. For χ being around $\chi_{k_0}^H$, the eigenvalue of (4.6) are $\sigma_1(\chi, k)$ and $\sigma_{2,3}(\chi, k) = \lambda(\chi, k) \pm i\tau(\chi, k)$. According to Theorem 2.13 in [22], $l(s)$ and $s\chi'_{k_0}(s)$ have the same zeros in small neighbourhood of $s = 0$ in which $l(s)$ and $-\lambda'(\chi_{k_0}^H)s\chi'_{k_0}(s)$ are of the same sign (if they are not zero), and

$$|l(s) + \lambda'(\chi_{k_0}^H)s\chi'_{k_0}s(s)| \leq |s\chi'_{k_0}(s)|o(1), \text{ as } s \to 0.$$

Then according to Theorem 8.23 in [34], the periodic orbits are stable if $l(s) > 0$, and are unstable if $l(s) < 0$. Because $\lambda(\chi_{k_0}^H) < 0$, and $l(s)$ and $s\chi'_{k_0}(s)$ have the same sign, one finds that supercritical branching solutions are stable and subcritical branches are unstable. Therefore, one need to compute χ'_{k_0} and/or χ''_{k_0} similar as above. The calculations using the factorization theorem in [38, 39] are straightforward but complicated hence skipped here.

In summary, we have proved the following theorem:

Theorem 4.2. *Suppose that all the conditions in Theorem 4.1 are satisfied and let $\vartheta_k(s) = \{(A_k(s,k), \rho_k(s,k), u_k(s,k), \chi_k(s))\}$, $k \in \mathbb{R}^+$ be the bifurcation branches given by (4.1). Denote $\chi_0 = \min_{k\in\mathbb{N}^+}\{\chi_k^S, \chi_k^H\}$ as in (2.7). Then the following hold:*

(i) If $\chi_0 = \chi_{k_0}^H < \min_{k\in\mathbb{N}^+}\chi_k^S$, then $\vartheta_{k_0}(s)$ around $(\bar{A}, \bar{\rho}, \bar{u}, \chi_{k_0})$ is asymptotically stable for $\chi''_{k_0}(0) > 0$ and it is unstable for $\chi''_{k_0}(0) < 0$, while $\vartheta_k(s)$ around $(\bar{A}, \bar{\rho}, \bar{u}, \chi_k)$ is always unstable for each $k \neq k_0$;

(ii) If $\chi_0 = \chi_{k_1}^H < \min_{k\in\mathbb{N}^+}\chi_k^S$, then $\vartheta_k(s)$ around $(\bar{A}, \bar{\rho}, \bar{u}, \chi_k)$ is always unstable for each $k \in \mathbb{N}^+$.

5 Numerical Simulations and Discussion

In this section we present results from several numerical studies of the evolutionary system (1.1) to demonstrate the formation of time-stationary and time-periodic criminal activities. Our numerical experiments examine the stability of the stationary and time-periodic spatially inhomogeneous solutions established in our theoretical analysis with $L = \pi$. We focus on

the effects of the hotspot policing intensity, measured by parameter χ, on the spatio-temporal dynamics of the coupled quantities. As mentioned earlier, we shall call the policing on-hotspot when $\chi = 2$, and the rest of the strategies off-hotspot. We point out that the off-hotspot policing has two subcategories depending on the sign of χ. In particular, we call it the anti–hotspot policing when $\chi < 0$, and this describes the choice that the police patrol areas that are not victimized instead of where crime density is high. Our numerical studies of the system will shed light on the spatio-temporal dynamics of criminal activities under the anti-hotspot policing and provide an academic comparison between these patrolling policies.

There are a few important observations we can make from these numerical simulations. First of all, this system of partial differential equations has an extremely rich and complicated spatio-temporal dynamics, besides those ruled by our rigorous theoretical steady-state and Hopf bifurcation analysis. Moreover, the dynamics turn out to be sensitive to the variation of system parameters, which make them intriguing from a mathematical analysis point of viewpoint. Second, all of our numerical studies begin with a small perturbation of the homogeneous solution. This choice is made to verify our theoretical findings and suggests a higher complexity within this system when even parsimonious initial data are allowed. Finally, as mentioned in the introduction, α and β are set constant in the mathematical modeling, and we will see how their magnitudes induce the variation of the spatio-temporal dynamics of the system.

5.1 On-spot policing with $\chi = 2$

In this section, we study on-spot policing of system (1.1) with $\chi = 2$. Our numerical studies begin with the formation of stable stationary hotspots demonstrated in Figures 2-4. In these simulations, we set $D_A = 0.01$, $\alpha = \beta = 1$, $\chi = 2$, and the initial data are chosen to be random and small perturbations from the homogeneous state $(\bar{A}, \bar{\rho}, \bar{u}) = (1.6180, 0.3820, 1)$:

$$(A_0, \rho_0, u_0) = (\bar{A}, \bar{\rho}, \bar{u}) + 0.01 \times \textbf{Random},$$

where **Random** is a 3×1 random vector, each with a length less than one.

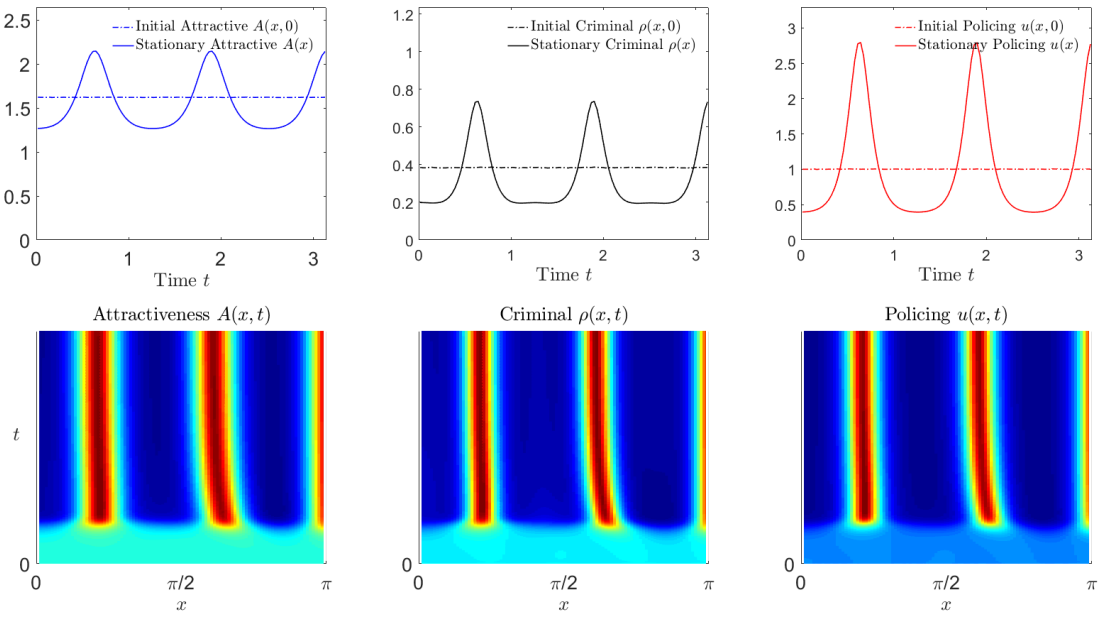

Figure 2: Formation of stable hotspots in $(0, \pi)$ out of small and random perturbation from the homogeneous state $(\bar{A}, \bar{\rho}, \bar{u}) = (1.6180, 0.3820, 1)$ under on-spot policing with $\chi = 2$. The rest system parameters are chosen as $D_A = 0.01, D_\rho = D_u = 0.5$ and $\alpha = \beta = 1$. The numerics find that this homogeneous solution loses its stability and develops into multiple spatial aggregates in the long time. These aggregates qualitatively describe the clustering in criminal hotspots.

Then we shrink diffusion rates $D_\rho(=D_u)$ from 0.5 in Figure 2 and 0.1 in Figure 3, to 0.05 in Figure 4. According to Proposition 2.1, the constant solution is unstable in all the three Figures, and this is numerically demonstrated here. Figure 2 serves as the benchmark that we test the effect of diffusion rates on the dynamics under the on-spot policing. We find that this homogeneous solution $(\bar{A}, \bar{\rho}, \bar{u}) = (1.6180, 0.3820, 1)$ develops into stable multiple spatial aggregates in the long time. One thing of note is that the number of aggregates, or hotspots, increases as the diffusion rates shrink. From the physical point of view, Figures 2-4 illustrate that even when parameters are spatially independent, *i.e.* the base attractiveness level is spatially homogeneous, crime seems to be concentrated in certain spatial locations. Asymmetric spikes are observed in Figure 4 when the diffusion rates are small, and such profiles are studied by [44] concerning system (1.1) without law enforcement.

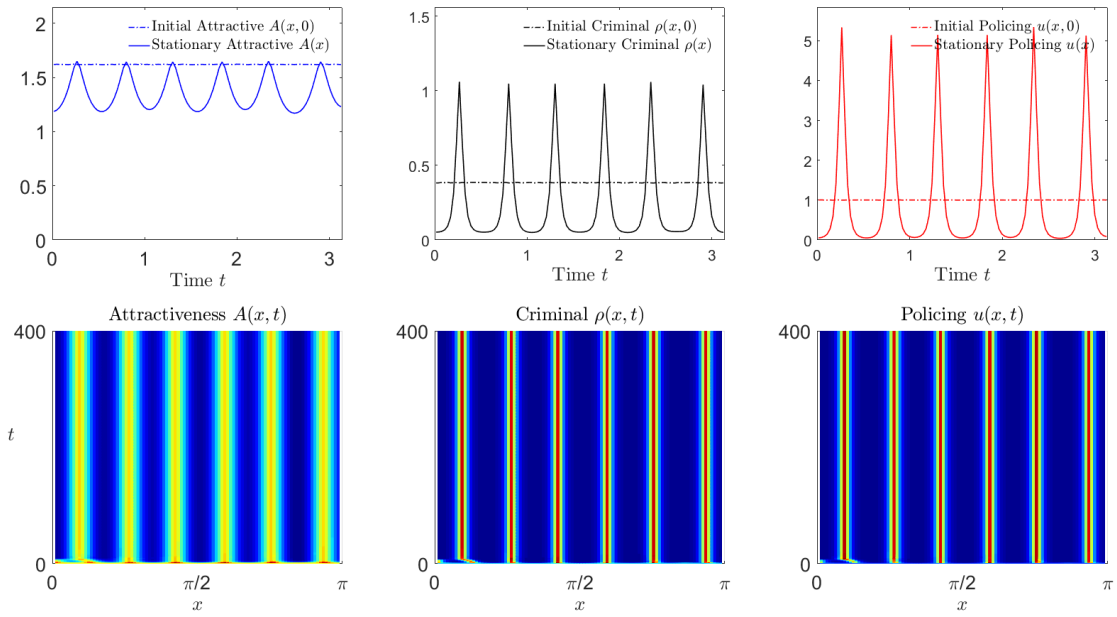

Figure 3: Formation of stable hotspots under on-spot policing with $\chi = 2$. The initial data and system parameters are the same as in Figure 2 except that $D_\rho = D_u = 0.1$. The numerics also find that this system develops criminal hotspots, and more aggregates for smaller diffusion rates. We would like to comment that, although the weakly nonlinear analysis presented in this paper only predicts the emergence of small-amplitude stable steady-state solutions, numerical simulations here indicate that these bifurcating solutions lead to large amplitude spike-type patterns along the solution branch. This comment applies further to time-periodic solutions as we shall see later.

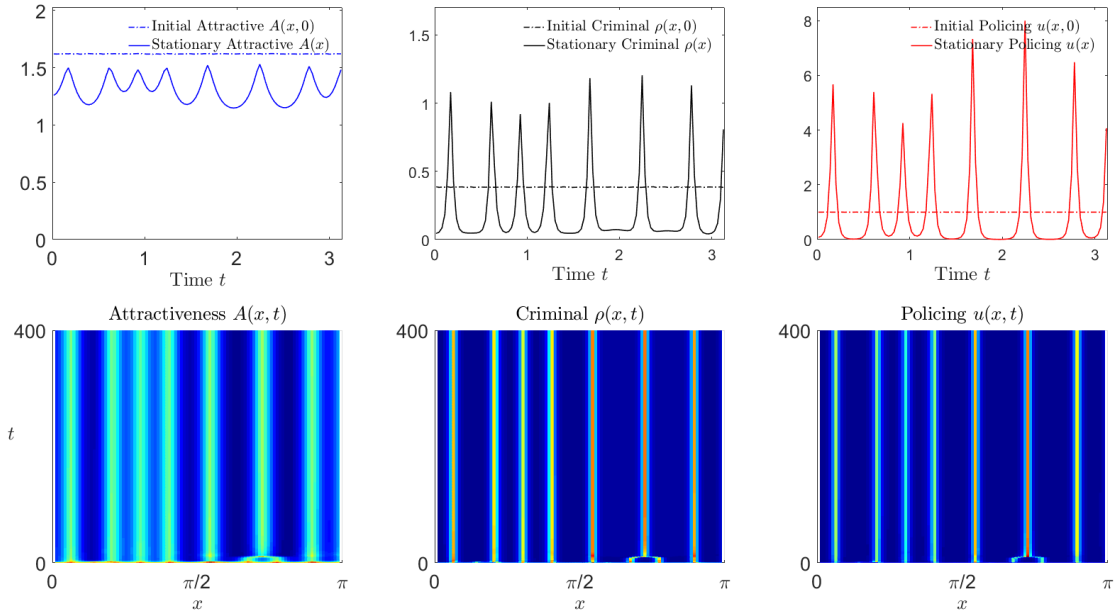

Figure 4: Formation of stable asymmetric hotspots under on-spot policing with $\chi = 2$. Again we choose the same initial data and parameters as in Figure 2 except that $D_\rho = D_u = 0.05$. More irregular and asymmetric criminal hotspots emerge as diffusivity further shrinks. These spiky patterns are beyond the analytical scope of this paper, whereas bifurcation from spikes is studied by [15, 73]

We next study the formation of time-periodic hotspot within system (1.1). In Figure 5, we present the formation and development time-oscillating hotspots out of the constant equilibrium $(0.0117, 0.1483, 1)$. Here the system parameters are $\alpha = 0.01, \beta = 0.15$, $D_A = 0.05$, $D_\rho = D_u = 0.05$ such a Hopf bifurcation occurs according to Theorem 4.2. The solution gradually decays to the constant solution for an extremely long time during the transient dynamics and then the amplitudes expand and the solution develops into stable time-periodic patterns for time t larger than 300. We would like to note that these oscillating patterns have small amplitude as they are small perturbations of the homogeneous solution.

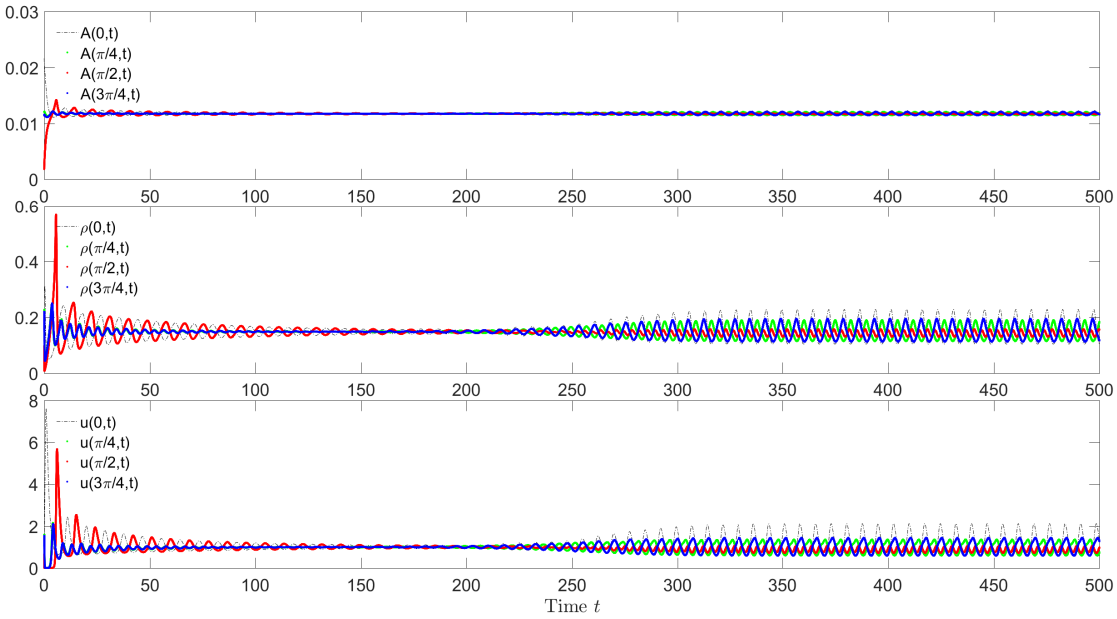

Figure 5: Formation of time-oscillating hotspots under on-spot policing out of small and random perturbation of the homogeneous state $(\bar{A}, \bar{\rho}, \bar{u}) = (0.0117, 0.1483, 1)$. The system parameters are $\alpha = 0.01, \beta = 0.15$, $D_A = 0.05$, $D_\rho = D_u = 0.05$ such the Hopf bifurcation occurs according to Theorem 4.2. They give rise to small-amplitude time-periodic solutions accordingly.

Figure 6 demonstrates the formation of large-amplitude, time-periodic hotspots for a different set of system parameters, but also out of the constant solution. We observe that the spiral dynamics around the constant solution endure for a long time. The dynamics then accelerate after $t > 50$ to develop a stable oscillates at around $t \approx 150$, through a phase transition at around $t \approx 100$. The phase transition between periodic loops is better illustrated within plots of Figure 7, which, for a fixed spatial location, illustrates the pair-wise oscillations of the unknowns. Note that the darker regions represent areas where the solutions spend more time and the less dense regions correspond to the phase transition. Furthermore, larger limiting cycles correspond to a wider oscillation in the solutions. Contrary to the previously discussed case, in this situation the crime density alternates in most locations in a time-periodic way. An interesting observation is that the areas with the highest amount of crime at some point are also the places with the lowest amount in others; see Figure 6 for an illustration of this.

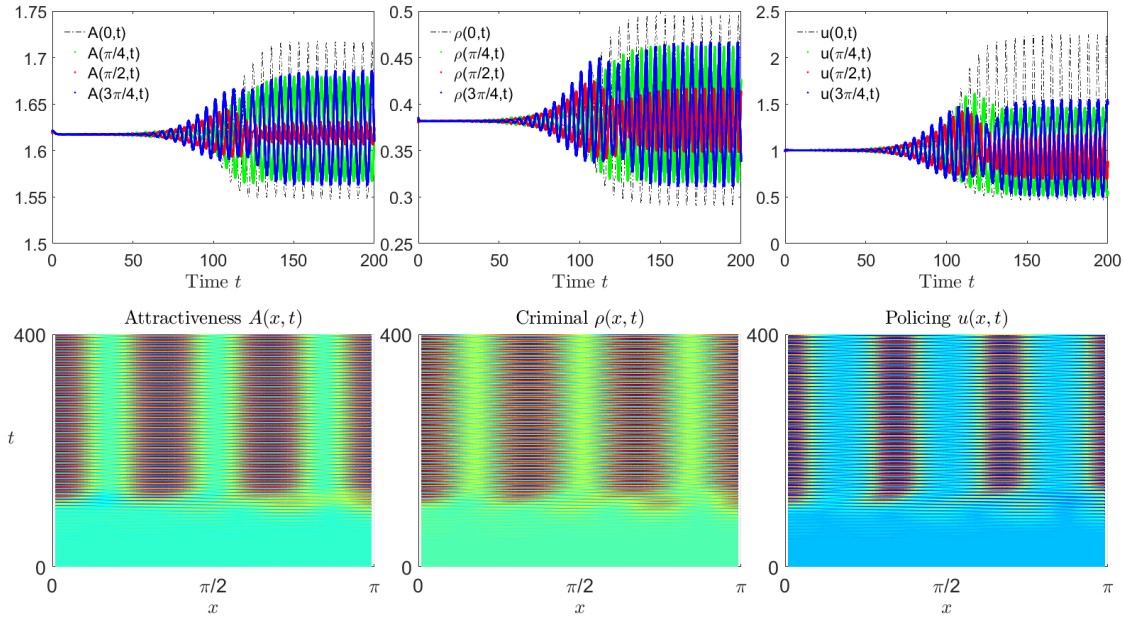

Figure 6: Formation of time-periodic hotspots under on-spot policing out of small and random perturbation of the homogeneous state $(\bar{A}, \bar{\rho}, \bar{u}) = (1.6180, 0.3820, 1)$. The system parameters are chosen to be $D_A = 0.1, D_\rho = D_u = 0.05$ and $\alpha = \beta = 1$. The numerics find that this homogeneous solution loses its stability and develops into time-periodic aggregates with large amplitudes in the long term.

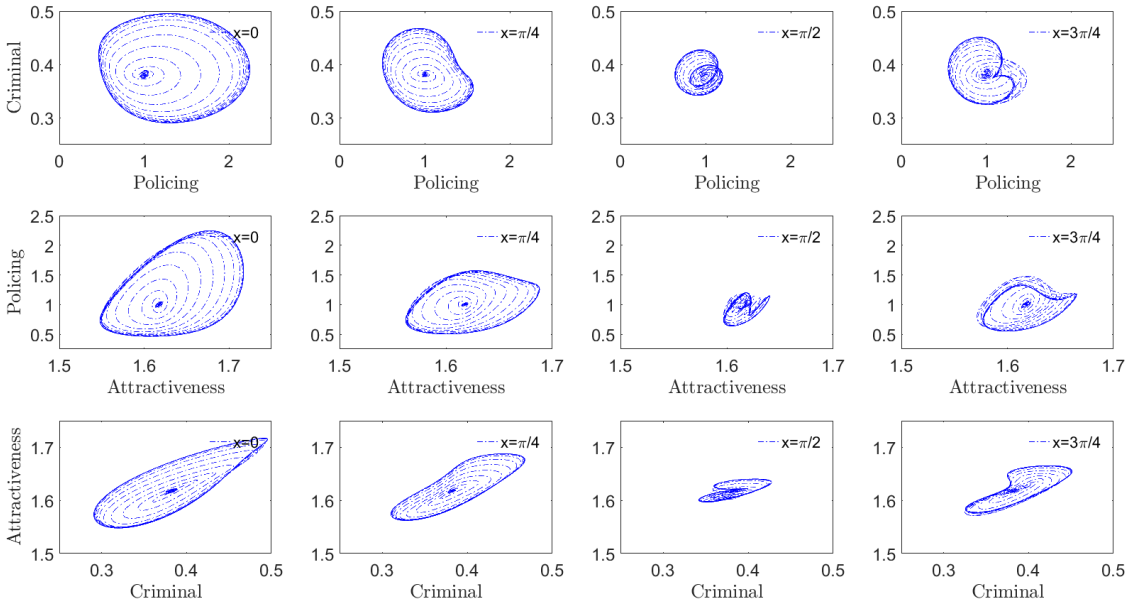

Figure 7: The pair-wise oscillations of the criminal, policing and attractiveness demonstrated within Figure 6 at fixed locations $x = 0, \pi/4, \pi/2$ and $3\pi/4$. The phase transition between loops are presented within the orbits.

In Figure 8, we continue to vary the system parameters to showcase another set of large-amplitude periodic solutions. These numerical experiments suggest that these large-amplitude profiles occur from a second bifurcation, not from the nonconstant solutions, which our analysis does not cover.

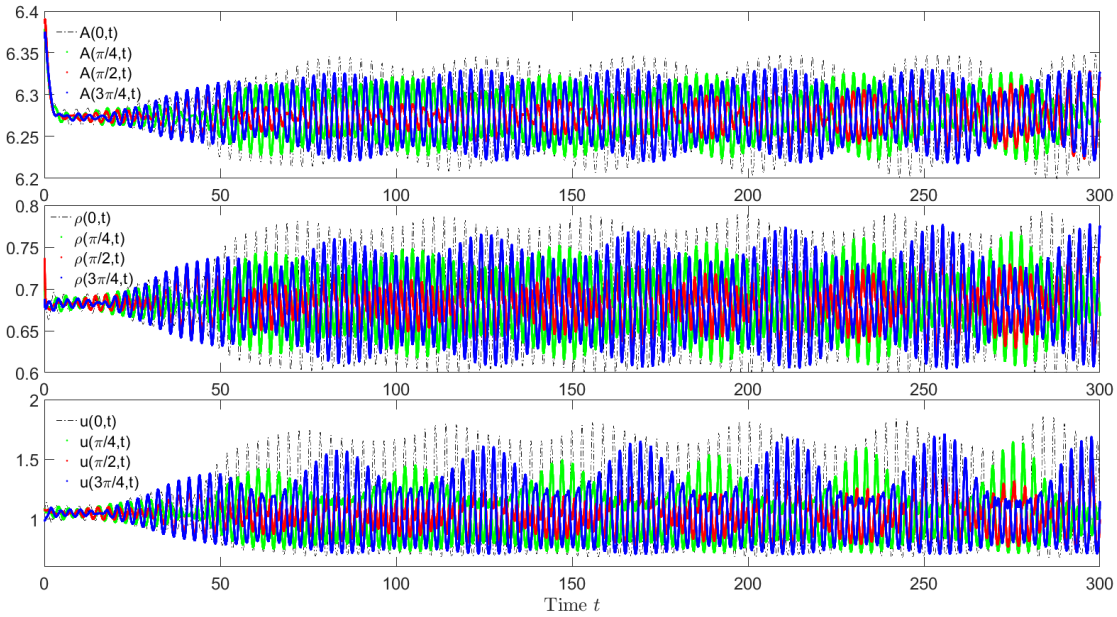

Figure 8: Time-periodic patterns with large amplitudes from the homogeneous state $(\bar{A}, \bar{\rho}, \bar{u}) = (1.6180, 0.3820, 1)$. The other parameters are chosen to be $D_A = 0.1579, D_\rho = D_u = 0.005$ and $\alpha = 1.99, \beta = 5$ and $\chi = 2$. The numerics suggest that a bifurcation occurs from the spatially inhomogeneous solutions whose analysis lacks.

The stationary and time-periodic patterns shown above not only illustrate our mathematical analysis but also provide evidence of rich spatio-temporal dynamics of this system which is perhaps more important from the viewpoint of mathematical modeling. Though a thorough analysis of these dynamics is far from complete, the long-time regularities developed therein provide some promises for further mathematical investigations of this system under those parameter regimes. However, we conclude this section by presenting additional numerical experiments that suggest the system dynamics might be impossible to investigate in other parameter regimes, which make the mathematical studies of the system intrigue, even under the on-spot policing regime.

In Figure 9, we conduct an experiment when the parameters are away from the bifurcation points. In particular, we choose $D_A = 0.1$, $D_\rho = D_u = 0.005$ and $\alpha = \beta = 1$, and the initial data be small perturbation from the constant solution, which is unstable. However, we find that, rather than developing into the seemingly dominating time-stationary or time-periodic patterns seen above, the dynamics endure a rather coarse and chaotic process, and the irregularity remains throughout the time of the simulation. They are well presented in the bottom figure which plots the evolution of L^2 distance between the solution and initial data. The irregularities are also presented by the pair-wise dynamics in Figure 10 as compared to their regular counterparts in Figure 7. These provide a piece of strong numerical evidence on the ill-posedness and chaos of the proposed system. We would like to mention that spatio-temporal patterns of these kinds (with oscillations or chaos) have been numerically in reaction-advection-diffusion system by various authors, e.g., [27, 37, 46, 53] on Keller–Segel models with cellular growth, and [75, 77] for predator-prey models with prey-taxis.

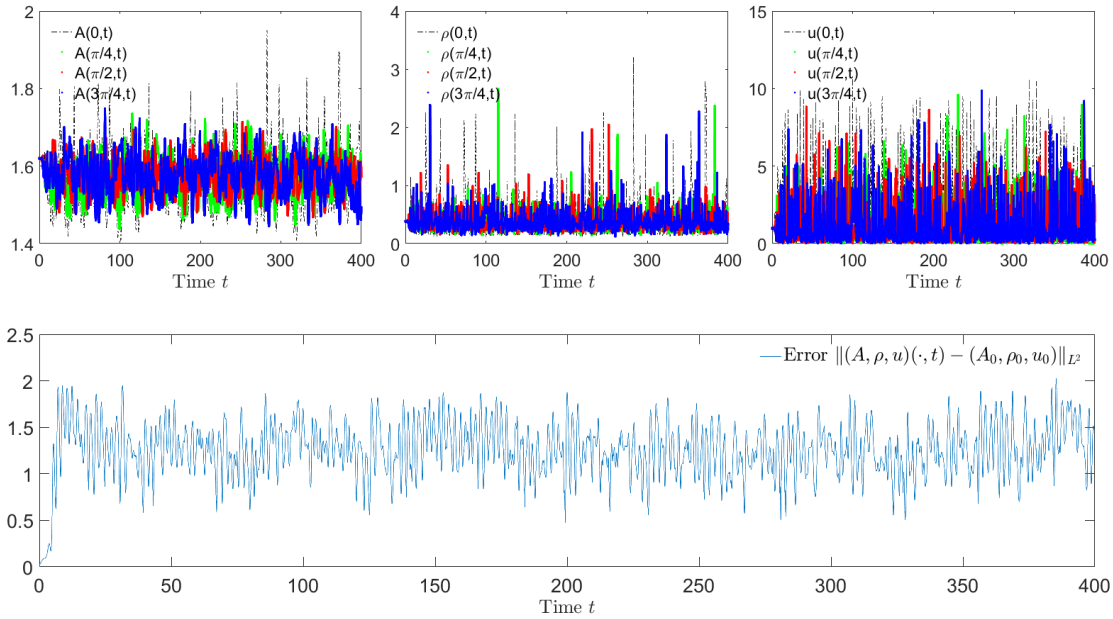

Figure 9: The chaotic oscillations demonstrated within the system for $\chi = 2$. The rest parameters are $D_A = 0.1$, $\alpha = \beta = 1$, and we shrink the diffusion rates $D_\rho = D_u$ from 0.05 to 0.005. The top presents the pointwise irregularities within the system and the bottom describes the irregular L^2-distance between the time-dependent solution and the initial data. These dynamics indicate that decreasing the criminal and police diffusivity further tends to introduce highly intricate and irregular oscillations into the system evidenced by a positive Lyapunov exponent.

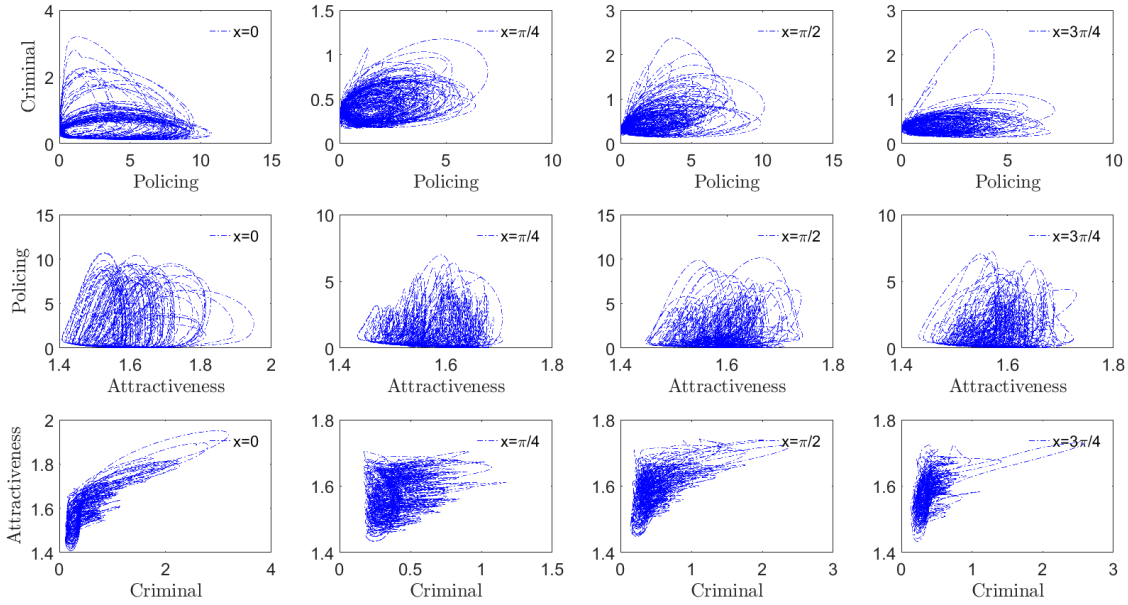

Figure 10: The pair-wise dynamics demonstrated within Figure 9.

We conduct another experiment in Figure 11 by varying α from 1 to 0.1, with the rest parameters fixed. Again we observe the formation of irregular patterns out of the constant solution. These findings, besides those not reported here, present a wide range of system parameters at which system (1.1) is ill-posed.

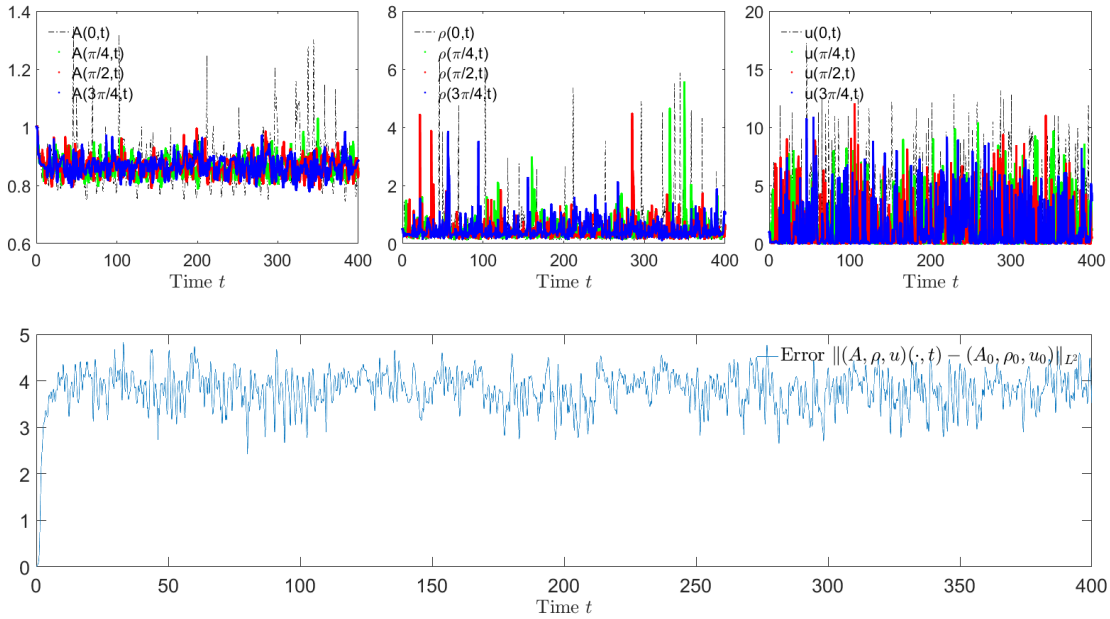

Figure 11: The chaotic oscillations demonstrated within the system for $\chi = 2$. The rest parameters are $D_A = 0.1$, $D_\rho = D_u = 0.005$, $\alpha = 0.5$ and $\beta = 1$. That is, we shrink α from 1 to 0.5.

It is necessary to mention that, we have informally said that these system "chaotic" because of their apparent spatio-temporal chaos. However, to justify this rigorously one would need to quantify the rate of separation of infinitesimally close trajectories by the Lyapunov exponent.

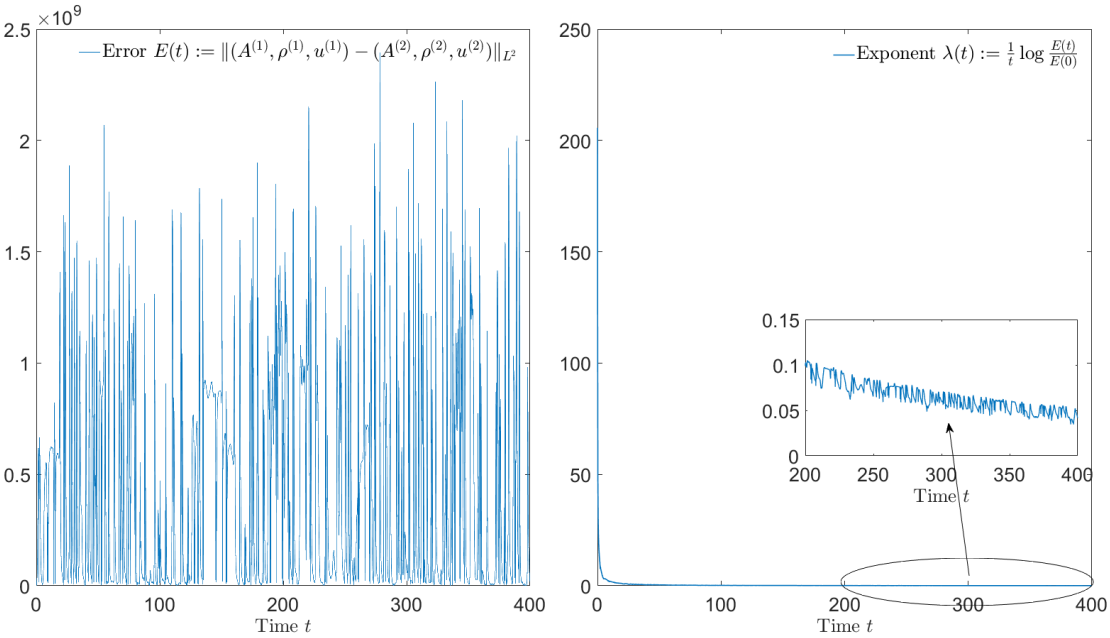

Figure 12: The distance between solutions out of two initial data with small perturbation. The Lyapunov exponent $\lambda(t)$ within the dynamics of Figure 11.

In Figure 12, we illustrate the Lyapunov exponent computed as the following

$$\lambda = \lim_{t\to\infty} \lambda(t), \text{where } \lambda(t) := \frac{1}{t}\log\frac{E(t)}{E(0)},$$

where $E(t)$ is the L^2 error between two infinitesimally-perturbed initial data $(A^{(1)}, \rho^{(1)}, u^{(1)})$ and $(A^{(2)}, \rho^{(2)}, u^{(2)})$

$$E(t) := \|(A^{(1)}, \rho^{(1)}, u^{(1)}) - (A^{(2)}, \rho^{(2)}, u^{(2)})\|_{L^2}.$$

Then we find that the L^2 error explodes to up to 10^9 even out of an infinitesimal perturbation. Our numerical simulation tends to suggest that $\lambda(t)$ approaches $\lambda \approx 0.03$, though again rigorous analysis is not a tool that we possess. In practice, a time horizon of up to $T = 400$ has been a good approximation of infinity hence the chaos is expected up to this time horizon.

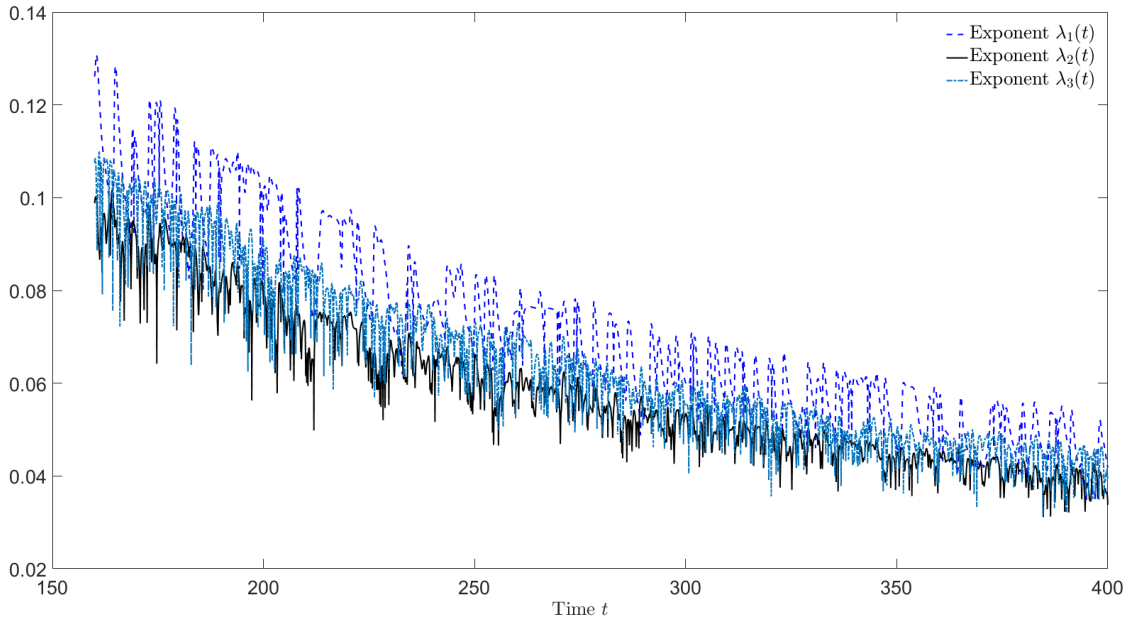

Figure 13: Lyapunov exponents $\lambda(t)$ of several random initial data.

Finally, we conduct three more tests in Figure 13 which support this observation. In summary, the chaos and ill-posedness are rampant within (1.1) across system parameters and initial data. These numerical experiments have important consequences from the point-of-view of application. Specifically, it cautions against the use of system (1.1) with the incorporation of data as a potential predictive tool, due to how sensitive the behavior of the solutions are to the system parameters.

5.2 Off-spot Policing with $\chi \neq 2$

We next present the numerics on the effect of off-spot policing with $\chi \neq 2$. In Figures 14-15, we choose $D_A = D_\rho = D_u = \alpha = \beta = \bar{u} = 1$, and have from above arguments that the constant solution $(\bar{A}, \bar{\rho}, \bar{u}) = (1.6180, 0.3820, 1)$ is locally stable for $\chi \in (-14.9443, 163.7345)$, and is unstable otherwise. This is examined numerically. For instance, Figure 14 readily presents the spiral convergence towards the constant solution in the long time, which tends to suggest that a spiral divergence occurs as χ surpasses 163.7345. This has been rigorously proved by our Hopf bifurcation theorems above and is now numerically tested in Figure 15 that we choose $\chi = 165$. The top three plots of Figure 15 present the formation and development of stable time-periodic patterns, and the bottom is the zoomed-in plot that gives a slightly detailed configuration of the dynamics.

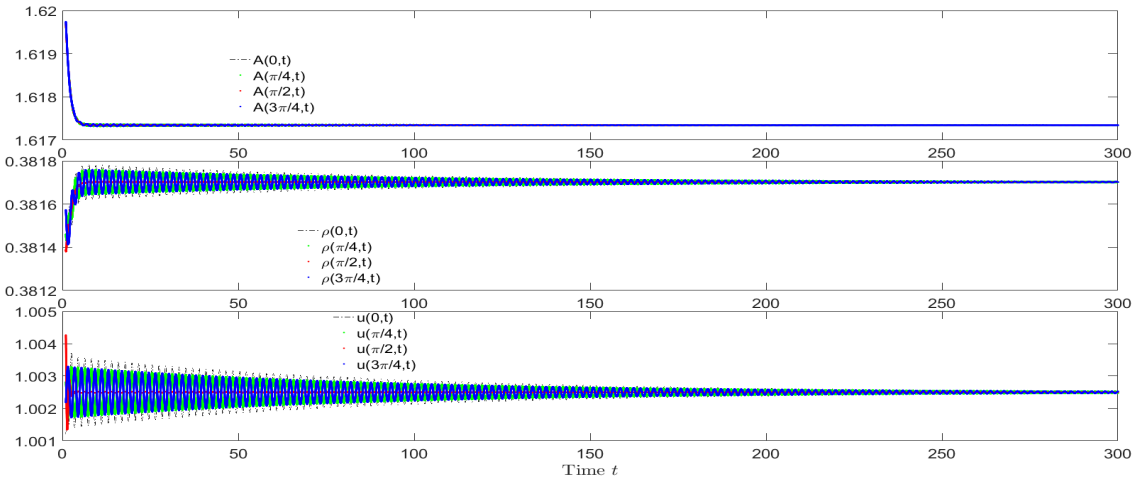

Figure 14: Demonstration of spiral convergence to the constant solution with $\chi = 160 \in (\chi^-, \chi^+)$. According to Proposition 2.1, $(\bar{A}, \bar{\rho}, \bar{u})$ is stable, and here we choose the points $x = 0, x = L/4, L/2$ and $3L/4$ to illustrate the spiral convergence to the constant, and the same behaviors are observed for all points. Parameters are chosen to be $D_A = D_\rho = D_u = \alpha = \beta = \bar{u} = 1$.

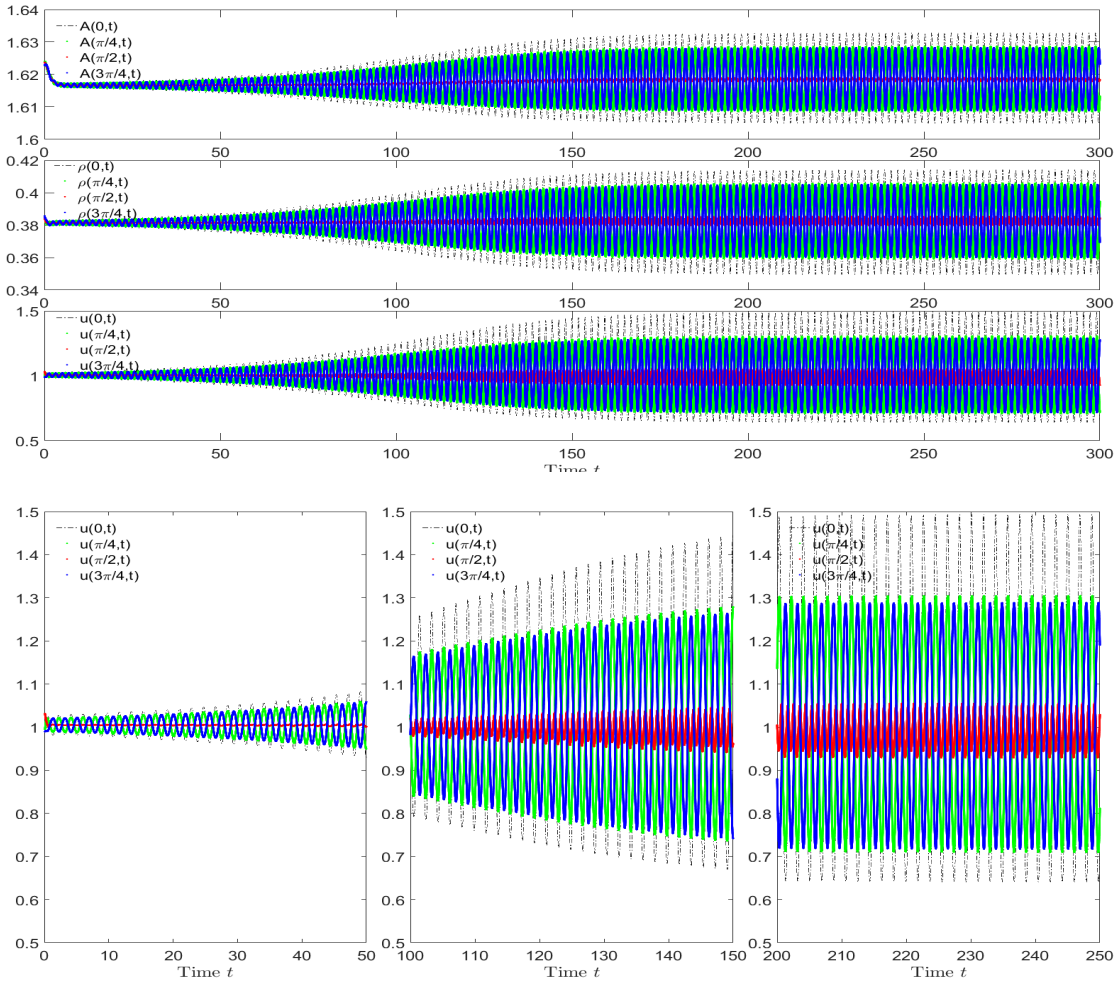

Figure 15: Formation of regular oscillating patterns as constant solution loses its stability. All parameters are chosen to be the same as those in Figure 12 except that we slightly increase χ to 165, for which the constant solution is unstable. The top, middle and bottom denote those of the $A(x,t)$, $u(x,t)$ and $\rho(x,t)$ at points $x = 0, x = L/4, L/2$ and $3L/4$.

In Figures 16-17, we provide another two sets of distinct parameters that support periodic patterns. Similarities and differences betweens them observe the transitional dynamics in the long time. In Figure 16, the solution spirally converges to the homogeneous state up to time $t \approx 20$, and then it diverges and stabilizes into a periodic solution after time $t \approx 50$. The dynamics within Figure 17 witness a transition from nodal convergence to spiral divergence.

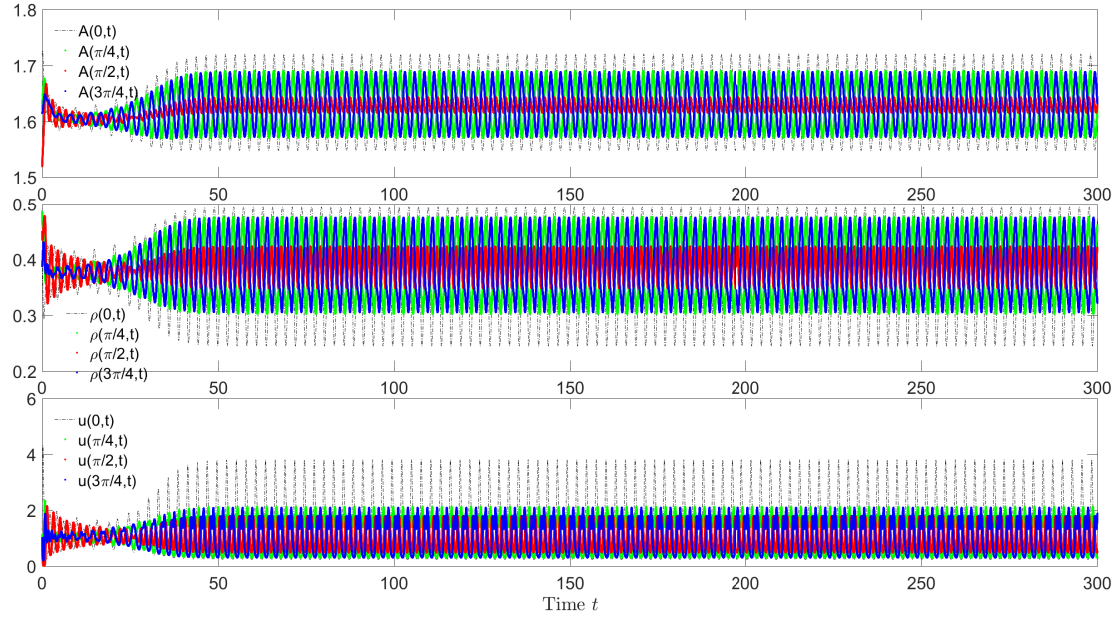

Figure 16: Formation of stable time-periodic patterns with large amplitude out of small perturbations from the constant solution $(\bar{A}, \bar{\rho}, \bar{u})$. Here the parameters are chosen $D_A = 0.01, D_\rho = 0.5, D_u = 0.5$, $\alpha = 1, \beta = 1$ and $\chi = 50$.

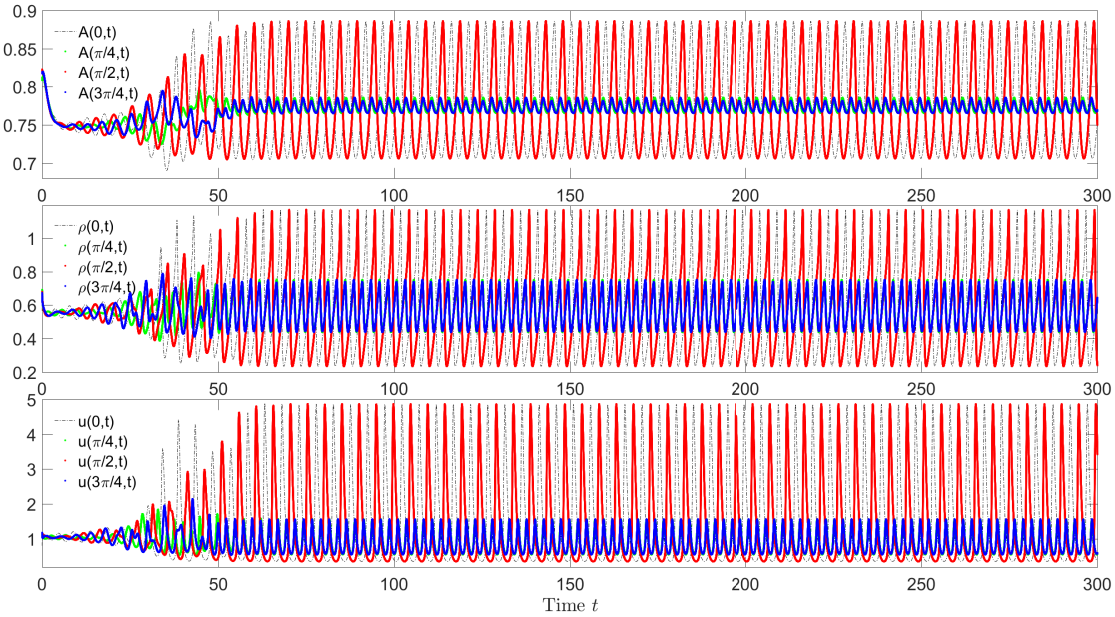

Figure 17: Formation of stable time-periodic patterns with large amplitude out of small perturbations from the constant solution $(\bar{A}, \bar{\rho}, \bar{u}) = (0.7653, 0.5665, 1)$. Here the parameters are chosen $D_A = 0.5, D_\rho = 0.01, D_u = 0.01$, $\alpha = 0.33175, \beta = 1$ and $\chi = 3$.

Figure 18 presents another interesting phase transition phenomenon within system (1.1). Here we choose $D_A = 1, D_\rho = 0.01, D_u = 0.01$, $\alpha = 1, \beta = 1$ and the $\chi = 47$ is away from Hopf bifurcation value. Starting with a small perturbation from the constant solution $(\bar{A}, \bar{\rho}, \bar{u}) = (1.6180, 0.3820, 1)$, the solution loses its amplitude and spirally converges to the constant solution to about $t = 100$. Then a phase transition occurs such that the solution gains momentum to develop its amplitude for yet another long process. The global dynamics are regular and mild all the time, and then they surprisingly explode to an orbit with proportionately large amplitude through another phase transition at $t \approx 400$ and develop into a stable periodic orbit after $t \geq 450$. The phase transitions are well presented in Figure 19, which nicely illustrates that the solutions remains close to the initial data for a very long time. These dynamics add another dimension in the challenges of the theoretical and numerical studies of the system.

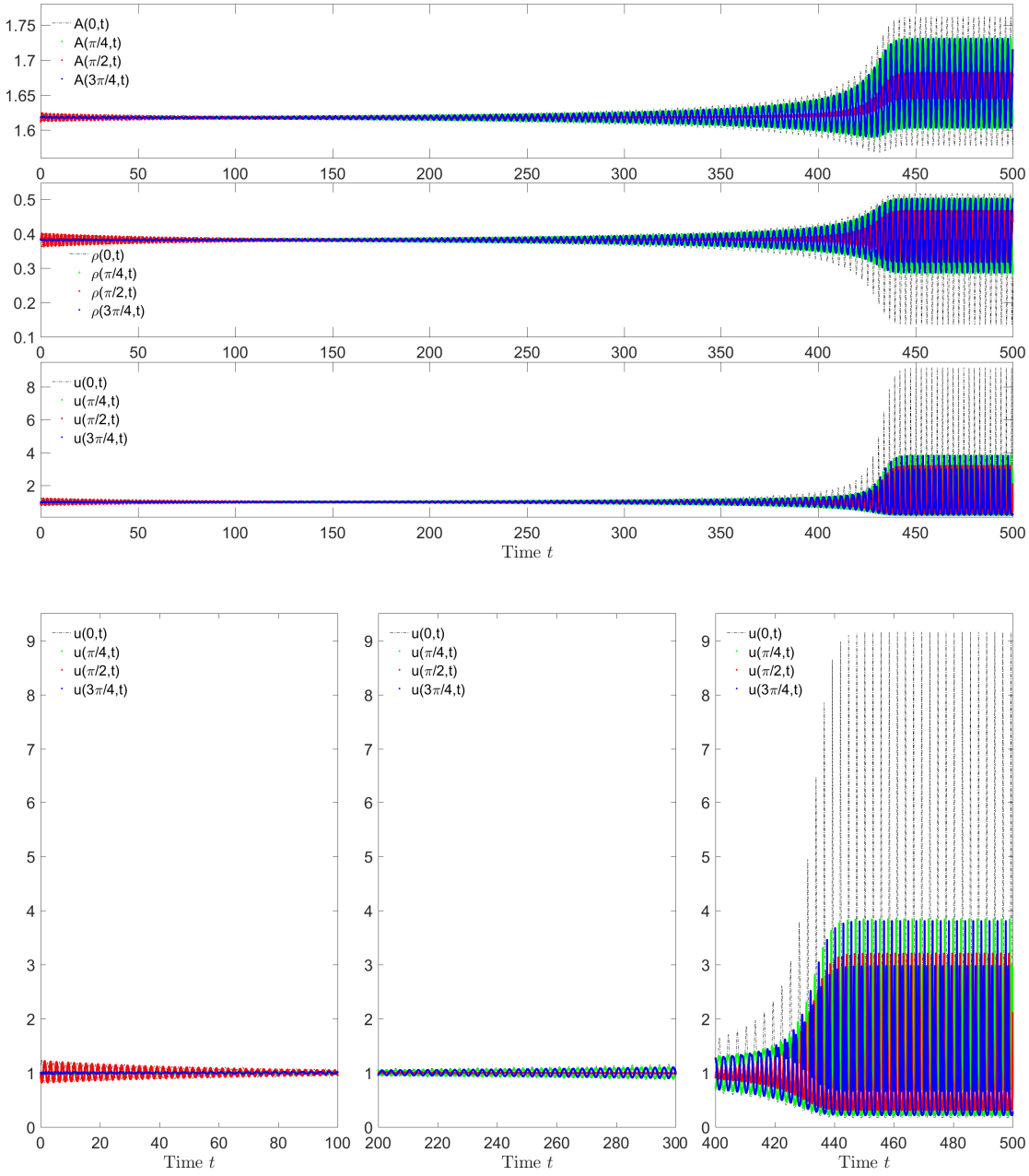

Figure 18: Formation of stable time-periodic patterns with large amplitude out of a small perturbation from the constant solution $(\bar{A}, \bar{\rho}, \bar{u}) = (1.6180, 0.3820, 1)$. Here the parameters are chosen $D_A = 1, D_\rho = 0.01, D_u = 0.01$, $\alpha = 1, \beta = 1$ and $\chi = 47$.

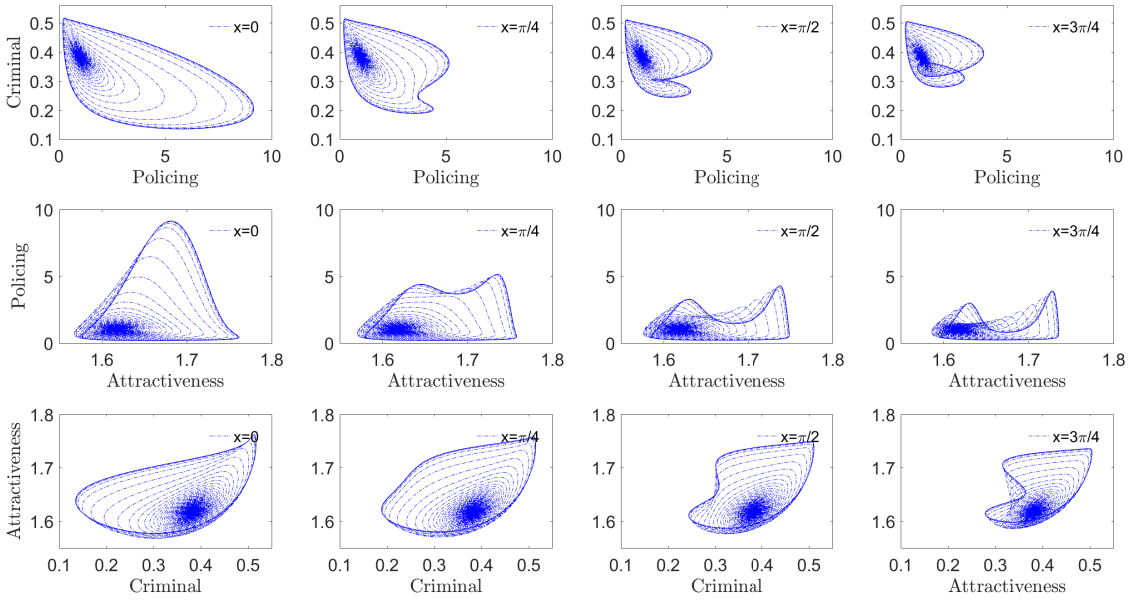

Figure 19: Pair-wise oscillations observed in Figure 18.

Finally, we examine in Figure 20 the effects of anti-hotspot policing on the dynamics of (1.1). Similarly as above, we choose the parameters $D_A = 0.1, D_\rho = D_u = 0.5$, $\alpha = \beta = 1$. Then we vary χ from -2, for which the constant solution is stable, to -5,-20 and -100. Our numerics suggest that the anti-hotspot policing preferably support stationary hotspots over time-periodic or chaotic patterns. Instead of driving hotspots to less attractive sites permanently or periodically, anti-hotspot policing tends to stabilize static spatial patterns and hotspots. As the anti-hotspot policing intensifies, stable hotspots with more aggregates emerge.

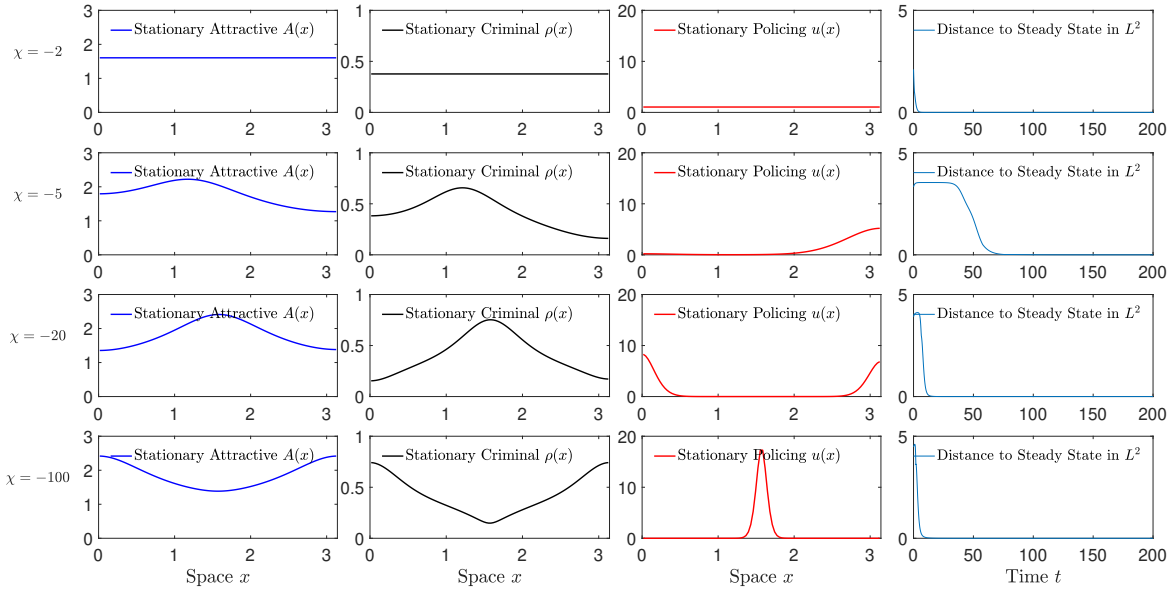

Figure 20: Effect of anti-hotspot policing on the formation of spatially inhomogeneous steady states out of small perturbations from the constant solution $(\bar{A}, \bar{\rho}, \bar{u}) = (1.6180, 0.3820, 1)$. $D_A = 0.1, D_\rho = D_u = 0.5$, $\alpha = \beta = 1$

5.3 Discussion and Future Works

This paper studies the effects on hotspot policing on the formation and development of both stationary and oscillating hotspot criminal activities in urban burglary. The main conclusion we draw from this study is the complex dynamic behavior of solutions to system (1.1), stemming from the inclusion of police dynamics. System (1.1) is thus a mathematically rich and compelling system to study. We have studied four parameter regimes leading to widely changing behaviors of the solutions. Most importantly, we point out that the parameter sensitivity of the system makes it difficult for system (1.1) to be used in practice. Also, the limits of the analytical framework preclude conclusions regarding whether enforcement-oriented programs result in long-term crime reductions in hot spot areas or crime in general. This work also offers little insight on the effectiveness of enforcement tactics relative to other broader-based community problem-solving policing programs (see, e.g. [3, 8, 72, 83]).

Due to the limitation of the analytical theory available, we cannot provide a complete picture of the system's dynamics. To study the qualitative behavior of the stationary or periodic solutions, one must characterize the continuum of bifurcation branches. However, current global bifurcation theories (e.g., [18, 66]) do not apply to our system due to the complex kinetics. We also note that the branches established in [16] are essentially local though global bifurcation is claimed. Indeed, we can not detect secondary bifurcations or predict the stability of the solution branches far from bifurcation points. This calls for a thorough numerical exploration of the bifurcation diagram using, for example, numerical bifurcation software, such as AUTO or MatCont in Matlab. Unfortunately, it is rarely possible to compute the Lyapunov exponent analytically, but some of the best algorithms for low-dimensional cases involve using a QR decomposition on the linearized dynamics, see for example [23]. It would also be of interest to compute the dimension of the attractor and also to visualize it, for example, using techniques from [19].

An appealing feature of system (1.1) is that under the assumptions that crime can happen anywhere and that all parameters are spatially and temporally homogeneous, we observe that crime tends to aggregate in certain areas, for certain parameters which are deemed physical. In a way, stating that while crime is aggregated, those aggregates do not discriminate based on geographic location. However, research suggests that a variety of situational factors cause crime to cluster at particular places and the model studied here ignores such factors. We find this to be a key limitation of the modeling framework used here and a key opportunity for potential future exploration. All the simulations are conduced with $L = \pi$, and similar (rich and complex) dynamics are observed but not reported here if the interval changes.

Furthermore, studies regarding the efficiency of hotspot policing depending on the type of criminal offense have been conflicting, and could be an area where modeling can provide some insight. For example, the authors of [11] found that hotspot policing worked best for drug offenses, violent crime and disorder, while it was less effective, but still had some positive effect, for property crimes. However, other works have concluded that hot spot policing worked best for the disorder, e.g. loitering, public drinking, solicitation, but was of limited use in dealing with violent offenses; see [26, 45, 63, 81]. Therefore, it is an interesting and important problem to understand the differences in these conclusions from a quantitative point of view. From the viewpoint of mathematical analysis, it is also interesting and important to rigorously study the ill-posedness of the system, which we have to leave open for future research.

References

[1] H. Amann, *Hopf bifurcation in quasilinear reaction-diffusion systems*, Delay Differential Equations and Dynamical Systems, Lecture Notes in Mathematics, 1475 (1991), 53-63.

[2] L. Anselin, J. Cohen, D. Cook, W. Gorr and G. Tita, *Spatial analyses of crime*, Criminal Justice, 4 (2000), 212-262.

[3] R. Barr and K. Pease, Crime placement, displacement, and deflection. In M. Tonry & N. Morris (Eds.), Crime and justice: A review of research, 12 (1990) 277-318.

[4] H. Berestycki, L. Mei and J. Wei, *The existence and stability of spike solutions for a chemotaxis system modeling crime pattern formation*, arXiv: 1911.10054.

[5] H. Berestycki and J.-P. Nadal, *Self-organised critical hot spots of criminal activity*, Eur. J. Appl. Math., 21 (2010), 371-399.

[6] H. Berestycki, N. Rodríguez and L. Ryzhik, *Traveling wave solutions in a reaction-diffusion model for criminal activity*, Multiscale Model. Simul., 11 (2013), 1097-1126.

[7] H. Berestycki, J. Wei and M. Winter, *Existence of symmetric and asymmetric spikes for a crime hotspot model*, SIAM J. Math. Anal., 46 (2014), 691-719.

[8] A. A. Braga, *Effects of hot spots policing on crime*, Annals of the American Academy of Political and Social Science, 578 (2001), 104-125.

[9] A. A. Braga, *Hot spots policing and crime prevention: A systematic review of randomized controlled trials*, Journal of Experimental Criminology, 1 (2005), 317-342.

[10] A. A. Braga, *Effects of hot spots policing on crime*, Campbell Systematic Reviews, 3 (2007), 1-36.

[11] A. A Braga, A. V. Papachristos and D. M. Hureau, *The effects of hot spots policing on crime: An updated systematic review and meta-analysis*, Justice Quarterly, 31 (2014), 633-663.

[12] A. A. Braga, D. L. Weisburd, E. J. Waring, L. G. Mazerolle, W. Spelman and F. Gajewski, *Problem-oriented policing in violent crime places: A randomized controlled experiment*, Criminology, 37 (1999), 541-580.

[13] A. A Braga, B. C. Welsh, C. Schnell, *Can policing disorder reduce crime? A systematic review and meta-analysis*, Journal of Research in Crime and Delinquency, 52 (2015), 567-588.

[14] P. Brantingham, *Domestic burglary repeats and space-time clusters the dimensions of risk*, Eur. J. Criminol., 2 (2005), 67-92.

[15] A. Buttenschoen, T. Kolokolnikov, M. Ward and J. Wei, *Cops-on-the-dots: the linear stability of crime hotspots for a 1-D reaction-diffusion model of urban crime*, European J. Appl. Math., 31 (2020), 871-917.

[16] R. Cantrell, C. Cosner and R. Manásevich, *Global bifurcation of solutions for crime modeling equations*, SIAM J. Math. Anal., 44 (2012), 1340-1358.

[17] S. Chaturapruek, J. Breslau, D. Yazdi, T. Kolokolnikov and S. McCalla, *Crime modeling with Lévy flights*, SIAM J. Appl. Math., 73 (2013), 1703-1720.

[18] A. Chertock, A. Kurganov, X. Wang and Y. Wu, *On a chemotaxis model with saturated chemotactic flux*, Kinet. Relat. Models, 5 (2012), 51-95.

[19] F. Christiansen, P. Cvitanović, V. Putkaradze, *Spatiotemporal Chaos in Terms of Unstable Recurrent Patterns*, Nonlinearity, 10 (1997), 55-70.

[20] M. G. Crandall and P. H. Rabinowitz, *Bifurcation from simple eigenvalues*, J. Funct. Anal., 8 (1971) 321-340.

[21] M. G. Crandall and P. H. Rabinowitz, *Bifurcation, perturbation of simple eigenvalues, and linearized stability*, Arch. Rational Mech. Anal., 52 (1973) 161-180.

[22] M. G. Crandall and P. H. Rabinowitz, *The hopf bifurcation theorem in infinite dimensions*, Arch. Rational Mech. Anal., 67 (1977) 53-72.

[23] L. Dieci, R.D. Russell, and E. van Vleck, *O*n the Compuation of Lyapunov Exponents for Continuous Dynamical Systems, SIAM J. Numer. Anal., 34 (1) (1997), 402-423,

[24] M. D'Orsogna and M. Perc, *Statistical physics of crime: A review*, Phys. Life Rev., 12 (2015), 1-21.

[25] J. Eck, Preventing crime at places. In L. Sherman, D. Farrington, B.Welsh, & D. L. MacKenzie (Eds.), Evidence-based crime prevention (pp. 241-294). (2002) New York: Routledge.

[26] J. Eck and D. Weisburd, (1995). Crime places in crime theory. In J. Eck & D. Weisburd (Eds.), Crime and place (pp. 1–34). Monsey, NY: Criminal Justice Press.

[27] S.I. Ei, H. Izuhara and M. Mimura, *Spatio-temporal oscillations in the Keller–Segel system with logistic growth*, Phys. D, 277 (2014), 1-21.

[28] M. Felsen,*Routine activities and crime prevention in the developing metropolis*, Criminology, 25 (1987), 911-932.

[29] M. Freitag, *Global solutions to a higher-dimensional system related to crime modeling*, Math. Methods Appl. Sci., 41 (2018), 6326-6335.

[30] M. García-Huidobro, R. Manásevich and J. Mawhin, *Solvability of a nonlinear Neumann problem for systems arising from a burglary model*, Appl. Math. Lett., 35 (2014), 102-108.

[31] E. R. Groff, S. D. Johnson and A. Thornton, *State of the art in agent-based modeling of urban crime: An overview*, J. Quant. Criminol., 35 (2019), 155-193.

[32] Y. Gu, Q. Wang and G. Yi, *Stationary patterns and their selection mechanism of urban crime models with heterogeneous near-repeat victimization effect*, European J. Appl. Math., 28 (2017), 141-178.

[33] F. Heihoff, *Generalized solutions for a system of partial differential equations arising from urban crime modeling with a logistic source term*, arXiv:1911.04838.

[34] D. Henry, Geometric theory of semilinear parabolic equations, Springer-Verlag-Berlin-New York (1981).

[35] T. Hillen and K. Painter, *A user's guide to PDE models for chemotaxis*, J. Math. Biol., 58 (2009), 183-217.

[36] D. Horstmann, *From 1970 until present: the Keller–Segel model in chemotaxis and its consequences I*, Jahresber DMV, 105 (2003), 103-165.

[37] L. Jin, Q. Wang and Z. Zhang, *Pattern formation in Keller–Segel chemotaxis models with logistic growth*, Int. J. Bifurc. Chaos, 26 (2016), 1650033-1–1650033-15

[38] D. D. Joseph and D. Nield, *Stability of bifurcating time-periodic and steady solutions of arbitrary amplitude*, Arch. Rational Mech. Anal., 58 (1975), 369-380.

[39] D. D. Joseph and D. H. Sattinger, *Bifurcating time periodic solutions and their stability*, Arch. Rational Mech. Anal., 45, (1972), 75-109.

[40] S. D. Johnson, K. Bowers and A. Hirschfield, *New insights into the spatial and temporal distribution of repeat victimization*, Br. J. Criminol., 37 (1997), 224-241.

[41] P. Jones, P. Brantingham and L. Chayes, *Statistical models of criminal behavior: The effects of law enforcement actions*, Math. Models Methods Appl. Sci., 20 (2010), 1397-1423.

[42] T. Kato, Functional Analysis, Springer Classics in Mathematics, 1995.

[43] E. F. Keller and L. A. Segel, *Model for chemotaxis*, J. Theoret. Biol., 30 (1971), 225-234.

[44] T. Kolokolnikov, M. Ward and J. Wei, *The stability of steady-state hot-spot patterns for a reaction-diffusion model of urban crime*, Discrete Contin. Dyn. Syst. Ser. B, 19 (2014), 1373-1410.

[45] C. Koper, *Just enough police presence: Reducing crime and disorderly behavior by optimizing patrol time in crime hot spots*, Justice Quarterly, 12 (1995), 649-672.

[46] K. Kuto, K. Osaki, T. Sakurai and T. Tsujikawa, *Spatial pattern formation in a chemotaxis–diffusion–growth model*, Phys. D, 241 (2012), 1629–1639.

[47] P. Liu, J. Shi and Z.-A. Wang, *Pattern formation of the attraction-repulsion Keller–Segel system*, Discrete Contin. Dyn. Syst. Ser. B, 18 (2013), 2597-2625.

[48] D. Lloyd and H. O'Farrell, *On localised hotspots of an urban crime model*, Phys. D, 253 (2013), 23-39.

[49] D. Lloyd, N. Santitissadeekorn and M. Short, *Exploring data assimilation and forecasting issues for an urban crime model*, European J. Appl. Math., 27 (2016), 451-478.

[50] R. Manásevich, M. Garcia-Huidobro and J. Mawhin, *Existence of solutions for a 1-D boundary value problem coming from a model for burglary*, Nonlinear Anal. Real World Appl., 14 (2013), 1939-1946.

[51] R. Manásevich, Q. Phan and P. Souplet, *Global existence of solutions for a chemotaxis-type system arising in crime modelling*, European J. Appl. Math., 24 (2013), 273-296.

[52] G. Mohler and M. Short, *Geographic profiling from kinetic models of criminal behavior.* SIAM J. Appl. Math., 72 (2012), 163-180.

[53] K. Painter and T. Hillen, *Spatio-temporal chaos in a chemotaxis model*, Phys. D, 240 (2011), 363-375.

[54] C. Pan, B. Li, C. Wang, Y. Zhang, N. Geldner, L. Wang and A. Bertozzi, *Crime modeling with truncated Lévy flights for residential burglary models*, Math. Models Methods Appl. Sci., 28 (2018), 1857-1880.

[55] G. Pierce, S. Spaar and L. Briggs, The character of police work: Strategic and tactical implications. Boston, MA: Center for Applied Social Research, Northeastern University, 1988

[56] A. Pitcher, *Adding police to a mathematical model of burglary*, European J. Appl. Math., 21 (2010), 401-419.

[57] L. Ricketson, A continuum model of residential burglary incorporating law enforcement, 2010.

[58] N. Rodríguez, *On the global well-posedness theory for a class of PDE models for criminal activity*, Phys. D, 260 (2013), 191-200.

[59] N. Rodríguez and A. Bertozzi, *Local existence and uniqueness of solutions to a PDE model of criminal behavior*, Math. Models Methods Appl. Sci., 20 (2010), 1425-1457.

[60] N. Rodríguez and M. Winkler, *On the global existence and qualitative behavior of one-dimensional solutions to a model for urban crime*, arXiv:1903.06331.

[61] J. Saldaña, M. Aguareles, A. Avinyó, M. Pellicer and J. Ripoll, *An age-structured population approach for the mathematical modeling of urban burglaries*, SIAM J. Appl. Dyn. Syst., 17 (2018), 2733-2760.

[62] R. Sampson and S. Raudenbush, *Seeing disorder: Neighborhood stigma and the social construction of broken windows*, Soc. Psychol. Q. 67 (2004), 319-342.

[63] J. Shaw, *Community policing against guns: Public opinion of the Kansas City gun experiment*, Justice Quarterly, 12 (1995), 695-710.

[64] L. Sherman, P. Gartin, and M. Buerger, *Hot spots of predatory crime: Routine activities and the criminology of place*, Criminology 27, (1989), 27-56.

[65] L. Sherman and D. Weisburd, *General deterrent effects of police patrol in crime "hot spots": A randomized, controlled trial*, Justice Quarterly 12 (1995), 625-648.

[66] J. Shi, X. Wang, *On global bifurcation for quasilinear elliptic systems on bounded domains*, J. Differential Equations, 246 (2009), 2788-2812.

[67] M. Short, A. Bertozzi and P. Brantingham, *Nonlinear patterns in urban crime: Hotspots, bifurcations, and suppression*, SIAM J. Appl. Dyn. Syst., 9 (2010), 462-483.

[68] M. Short, P. Brantingham, A. Bertozzi and G. E. Tita, *Dissipation and displacement of hotspots in reaction-diffusion models of crime*, P. Natl. Acad. Sci. USA, 107 (2010), 3961-3965.

[69] M. Short, M. D'Orsogna, V. Pasour, G. Tita, P. Brantingham, A. Bertozzi and L. Chayes, *A statistical model of criminal behavior*, Math. Models Methods Appl. Sci., 18 (2008), 1249-1267.

[70] M. Short, M. D'Orsogna, P. Brantingham and G. Tita, *Measuring and modeling repeat and near-repeat burglary effects*, J. Quant. Criminol., 25 (2009), 325-339.

[71] W. Skogan and K. Frydl, Fairness and effectiveness in policing: The evidence. Committee to Review Research on Police Policy and Practices. Washington, DC: The National Academies Press. (2004)

[72] W. Skogan and S. Hartnett, Community policing, Chicago style. New York: Oxford University Press. (1997)

[73] W.H. Tse and M. Ward, *Hotspot formation and dynamics for a continuum model of urban crime*, European J. Appl. Math., 27 (2016), 583-624.

[74] W.H. Tse and M. Ward, *Asynchronous instabilities of crime hotspots for a 1-D reaction-diffusion model of urban crime with focused police patrol*, SIAM J. Appl. Dyn. Syst., 17 (2018), 2018-2075.

[75] K. Wang, Q. Wang and F. Yu, *Stationary and time-periodic patterns of two-predator and one-prey systems with prey-taxis*, Discrete Contin. Dyn. Syst., 37 (2017), 505-543.

[76] Q. Wang, C. Gai and J. Yan, *Qualitative analysis of a Lotka-Volterra competition system with advection*, Discrete Contin. Dyn. Syst., 35 (2015), 1239-1284.

[77] Q. Wang, Y. Song and L. Shao, *Nonconstant positive steady states and pattern formation of 1D prey-taxis systems*, J. Nonlinear Sci., 27 (2017), 71-97.

[78] Q. Wang, D. Wang and Y. Feng, *Global well-posedness and uniform boundedness of urban crime models: One-dimensional case*, J. Differential Equations, 269 (2020), 6216-6235.

[79] Q. Wang, J. Yang and L. Zhang, *Time periodic and stable patterns of a two-competing-species Keller–Segel chemotaxis model effect of cellular growth*, Discrete Contin. Dyn. Syst. Ser. B, 22 (2017), 3547-3574.

[80] Q. Wang, L. Zhang, J. Yang and J. Hu, *Global existence and steady states of a two competing species Keller–Segel chemotaxis model*, Kinet. Relat. Models, 8 (2015), 777-807.

[81] D. Weisburd and J. Eck, *What can police do to reduce crime, disorder, and fear?*, Annals of the American Academy of Political and Social Science, 593 (2004) 42-65.

[82] D. Weisburd and L. Green, *Policing drug hot spots: The Jersey City drug market analysis experiment*, Justice Quarterly, 12 (1995), 711-735.

[83] D. Weisburd and L. Green, Measuring immediate spatial displacement: Methodological issues and problems. In J. Eck & D. Weisburd (Eds.), Crime and place (pp. 349–361). Monsey, NY: Criminal Justice.

[84] D. Weisburd, L. Maher and L. Sherman, *Contrasting crime general and crime specific theory: The case of hot spots of crime*, Advances in Criminological Theory 4, (1992), 45-69.

[85] J. Wilson and G. Kelling, *Broken windows: The police and neighborhood safety*, Atlantic Mon., 249 (1982), 29-38.

[86] M. Winkler, *Global solvability and stabilization in a two-dimensional cross-diffusion system modeling urban crime propagation*, Ann. Inst. H. Poincaré Anal. Non Linéaire, 36 (2019), 1747-1790.

[87] J. Zipkin, M. Short and A. Bertozzi, *Cops on the dots in a mathematical model of urban crime and police response*, Discrete Contin. Dyn. Syst. Ser. B, 19 (2014), 1479-1506.